energies

MDPI

Article

Energy and Economic Analysis of Technologies Suitable for Energy Transition in the Hospital Sector

Giulia Anna Maria Castorino, Lucrezia Manservigi *, Pier Ruggero Spina and Mauro Venturini

Department of Engineering, Università degli Studi di Ferrara, 44121 Ferrara, Italy; giuliaannamaria.castorino@unife.it (G.A.M.C.); pier.ruggero.spina@unife.it (P.R.S.); mauro.venturini@unife.it (M.V.)

* Correspondence: lucrezia.manservigi@unife.it

Abstract

The energy sector is currently facing the challenge of achieving energy transition targets while maintaining a reliable and economically sustainable energy supply. In this context, this study aims to identify the energy conversion technologies and storage systems that are expected to play a leading role in the hospital sector up to 2050. To this end, an optimization approach is developed to simultaneously optimize both the size and operation of a multi-generation energy system (MES) by means of the integration of two algorithms, i.e., particle swarm optimization and mixed-integer linear programming. The proposed approach is applied to a hospital hypothetically located in the city of Torino (Italy). For the considered projections, investments for future scenarios are profitable with NPV values up to 4.6 M€ and a discounted return on investment that is always positive in all the investigated cases. In addition, the initial investment is recovered well before the end of the MES' expected lifetime. An additional takeaway from this study is the sensitivity analysis that provides guidelines about the influence of both electricity price and fuel cost on investment profitability. Furthermore, the proposed optimization framework supports operational decision-making by identifying cost-effective sizing and management strategies under different future energy scenarios, thereby facilitating informed investment planning and contributing to the energy transition of hospitals.

Keywords: hospital energy demand; 2030 and 2050 scenarios; sizing and operation optimization; multi-generation energy system

1. Introduction

Nowadays the energy supply sector has to tackle ever-growing energy demands, while also upholding energy transition targets. Moreover, in many applications, the energy supply must be reliable, such as, for instance, in the hospital sector. Hospitals are highly energy-intensive buildings, which must be operational 24/7 every day of the year. In addition, the constant need for power supply, medical equipment, special air-quality requirements, and disease control means that their energy intensity is higher than that of other buildings in the tertiary sector [1,2].

The search for an optimized management strategy for hospitals has long been overlooked, despite the opportunities for energy savings and CO_2 emission reduction [3–5]. This is primarily due to the perception that patients must be provided with maximum comfort in all necessary conditions. Therefore, the implementation of new energy systems and management strategies must maintain the same level of comfort while achieving savings in

Check for updates

Academic Editor: Ammar Al-Bazi

Received: 14 July 2026
Revised: 9 September 2026
Accepted: 17 September 2026
Published: 22 September 2026

Copyright: © 2026 by the authors. Licensee MDPI, Basel, Switzerland. This article is an open access article distributed under the terms and conditions of the Creative Commons Attribution (CC BY) license.

energy consumption and emission reduction [5]. The health sector should indeed be an example by greening itself and reducing its ecological footprint [6].

Energy consumption in hospitals is often unreported in order to preserve the confidentiality of sensitive data. To this end, energy consumption can be determined as a function of the specific hours of operation [7], number of hospital beds, or hospital surface [1,8]. For example, the average yearly energy consumption of a healthcare center may be in the range of 86 kWh/m^2 [8] to 407 kWh/m^2 [9], the large majority of which is usually consumed for space heating [9].

Possible interventions in the outer envelopes of buildings and in the heating, cooling and lighting systems demonstrated that the reduction in energy consumption could be approximately 13% for heating energy and 62% for cooling energy.

The studies mentioned above highlight that hospital buildings have very high energy intensity levels and require continuous electricity supplies, heating, and cooling. Therefore, data consumption analysis allows us to enhance energy management [10]. In addition, an optimal sizing and operation strategy for energy technologies installed in healthcare facilities guarantees meeting their energy demand while also achieving economic and environmental benefits. Energy refurbishment may be an additional option to reduce the high level of energy consumption of healthcare facilities [11]; for example, an average yearly increase of 6% in time spent on preventive maintenance operations, over a period of five years, may result in a 20% decrease in the demand for corrective maintenance, and an average yearly saving of 10% in energy consumption [12]. The replacement of low-efficiency equipment can reduce energy consumption by 53.6% by employing a management strategy implemented by means of optimization algorithms [1].

A multi-generation energy system (MES) perfectly fits this scope, since it has the advantage of producing both power and heat at the same time, as well as meeting cooling energy demand by also achieving both energy and expenditure savings. Generally, a MES is a combination of two or more energy production, conversion, and storage systems, which interact with each other with the aim of meeting user energy demands. The advantages of MES implementation are mainly the energy, economic, and environmental benefits derived from both optimal MES sizing and management strategies [13–17]. In fact, a MES allows the integration of multiple energy carriers and energy conversion and storage technologies to create a resilient and flexible energy supply system, suitable for tertiary-sector infrastructure [18].

The paper contributes to the state of the art by identifying the energy conversion technologies and storage systems that are expected to play a leading role in hospital buildings in the years 2030 and 2050, also accounting for uncertainties in both fuel and electricity costs. In 2030, the MES is upgraded with respect to the current conventional plant, while in 2050 the entire MES is re-designed from scratch.

These goals are addressed by developing an optimization framework that simultaneously optimizes MES sizing and operation. It is worth noting that nested optimization approaches have been only marginally applied in the energy systems field, especially for simultaneous sizing and operation purposes (e.g., [15,19,20]). In this study, the particle swarm optimization (PSO) algorithm is used to identify the optimal size of MES components with the goal of maximizing the net present value (NPV), while the optimal MES operation strategy is identified by means of a mixed-integer linear programming (MILP) algorithm with the goal of maximizing the annual cash flow (ACF).

PSO is known for its straightforward implementation compared to other evolutionary algorithms like genetic algorithms. In fact, it requires fewer parameters to tune, which makes it easier to adapt and apply to different problems. In addition, PSO tends to converge faster to optimal or near-optimal solutions, especially in high-dimensional search spaces.

This makes this algorithm preferable to SMO, which suffers from the curse of dimensionality and thus requires a limited number of decision variables; in fact, a high number of decision variables could lead to degraded performance and unreliable optimization results [14,19]. PSO is highly flexible and can be easily adapted to different optimization problems by adjusting the velocity and position update rules. Furthermore, adaptive inertia weights help to balance both solution exploration and exploitation in the search space [21,22]. On the other hand, PSO requires higher computational time compared to SMO.

MILP is a robust optimization technique used to solve complex problems in various fields. Mixed-integer programming is a powerful tool for modeling and solving real-world planning and scheduling problems, for example, those related to system analysis and optimization in several applications. It is a state-of-the-art mathematical modeling technique for optimizing energy systems [13,23].

In conclusion, the proposed framework represents a practical decision-support tool for hospital energy managers and planners. By simultaneously optimizing system sizing and operational scheduling under different scenarios, it supports informed investment decisions while improving the long-term economic and operational sustainability of healthcare energy systems.

2. Methodology

The MES considered in this study can be equipped with several energy technologies: photovoltaic (PV) panels, a solar thermal collector (STC), a combined heat and power (CHP) system based on an internal combustion engine, a gas boiler (GB), an air source heat pump (ASHP), an absorption chiller (AC), a compression chiller (CC), thermal energy storage (TES) and battery energy storage (BES). The MES is connected to both the power grid (PG) and the fuel supply network. Each system is modeled using power and efficiency curves, accounting for the effects of ambient temperature and part-load operation, as described in [14].

The optimization procedure aims at the simultaneous optimization of both sizing and operation by means of the combination of two algorithms (Figure 1).

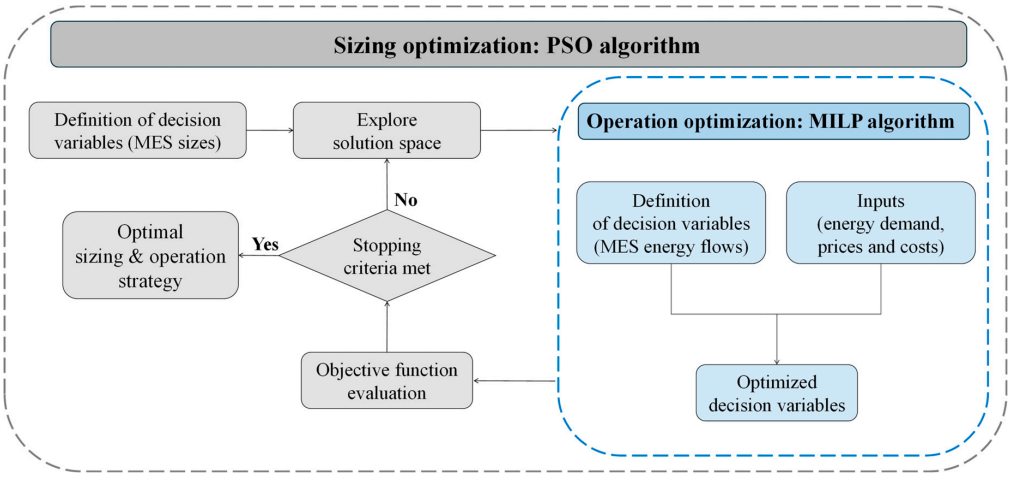


Figure 1. Sizing and operation optimization flowchart.

The operation optimization is nested within the sizing optimization with the aim of minimizing a specific objective function. The core idea consists of the concurrent use of the PSO algorithm, used to optimize MES technology sizes, and the MILP algorithm, which optimizes MES operation. This methodology combines the sizing optimization (outer level) with operation optimization (inner level) by means of the simultaneous identification of optimal variables for both sizing and operation. Sizing and operation optimization

are inherently connected and depend on each other. The identification of the optimal operating strategy depends on technology sizes since these define the energy supplied by the different energy systems. PSO handles the outer-level optimization, while the MILP algorithm addresses the inner-level optimization.

Figure 1 shows the flowchart of the optimization procedure. At each iteration, the PSO algorithm generates a combination of MES sizes (i.e., "Explore solution space" in Figure 1), for which the optimal operation strategy (i.e., MES energy flows, which are the decision variables of the MILP problem) is subsequently determined by the MILP algorithm. Integer-feasible solutions are identified using heuristic methods, and the optimal solution is searched ("Optimized decision variables" step in Figure 1). The objective function minimized by the PSO algorithm is then evaluated for the combination of MES sizes and its corresponding optimal operation strategy is determined by the MILP algorithm. If the stopping criteria are not satisfied (e.g., a predefined tolerance on the objective function value is not met), the PSO algorithm proceeds to the next iteration by updating the MES size and determining its optimal operation strategies. This iterative process continues until the stopping criteria are satisfied. Further details on the rationale underlying the use of the PSO and MILP algorithms can be found in [19,24].

Optimization is performed by considering an hourly time-step simulation for one year of operation.

2.1. Sizing Optimization

Sizing optimization is aimed at maximizing the PSO objective function, which in this study is the net present value (NPV). NPV is expressed in Equation (1): the total CAPEX accounts for the investment in new technologies, while the yearly cash flow (ACF) includes OPEX, expenditures for electricity supply from the PG, the expenditures for fuel, and the cost of CO_2 emissions. In addition, ACF also accounts for the revenues from electrical, thermal and cooling energy sold to users and the revenue of electrical energy sent to the PG, according to Equation (2). NPV is assessed over a period of ty years with a discount rate (DR). As reported in Equation (3), OPEX accounts for both fixed and variable components (i.e., FC and VC, respectively) of each MES technology. It has to be noted that, in Equation (2), the C values represent the total costs of electricity purchased from the grid, fuel, and CO_2 emissions. The variable $R_{\mathrm{Eel,sold}}$ includes both the revenue for electricity sold to the PG and the revenue for electricity sold to users, which are remunerated with different prices. In fact, the electricity sold to the user also accounts for taxes, network and distribution system costs. In addition, the revenue from thermal and cooling energy sold to users (i.e., $R_{\mathrm{Eth,sold}}$ and $R_{\mathrm{Ecool,sold}}$) is included.

$$\mathrm{NPV} = -\mathrm{CAPEX} + \sum_{\mathrm{n}=1}^{ty} \frac{\mathrm{ACF}}{(1+\mathrm{DR})^{\mathrm{n}}} \quad (1)$$

$$\mathrm{ACF} = -\mathrm{OPEX_{MES}} - C_{\mathrm{E_{el,from\ PG}}} - C_{\mathrm{fuel}} - C_{\mathrm{CO2}} + R_{\mathrm{E_{el,sold}}} + R_{\mathrm{E_{th,sold}}} + R_{\mathrm{E_{cool,sold}}} \quad (2)$$

$$\mathrm{OPEX_{MES}} = \mathrm{FC_{MES}} + \mathrm{VC_{MES}} \quad (3)$$

2.2. Operation Optimization

The operation optimization manages the energy flows between MES components and users to minimize the MILP objective function. In this work, the objective function is the ACF, defined in Equation (4):

$$\mathrm{ACF_{MILP}} = -\mathrm{OPEX_{MES}} - C_{\mathrm{E_{el,from\ PG}}} - C_{\mathrm{fuel}} - C_{\mathrm{CO2}} + R_{\mathrm{E_{el,sold}}} + R_{\mathrm{E_{th,sold}}} + R_{\mathrm{E_{cool,sold}}} \quad (4)$$

It must be noted that the definitions reported in Equations (2) and (4) are the same. However, Equation (2) is used to evaluate NPV, which is the objective function of PSO and is used for sizing optimization over the considered time period (*ty* years), while Equation (4) is the objective function of MILP and is used for operation optimization over one year.

The modeling framework, that allows the simulation of the technologies included in the MES, is reported below. We present the linear equations and linear constraints required for the technologies' implementation in the MILP algorithm.

At each time step t, electrical, thermal, and cooling energy demand must be met. Accordingly, Equations (5)–(7) allow satisfying such a constraint. CHP, PV, BES, and PG are employed to supply electrical energy; thermal energy demand can be met by CHP, GB, TES, ASHP, and STC, while CC, AC, and ASHP are used to supply cooling energy.

$$E_{\mathrm{CHP,el,t\rightarrow U}} + E_{\mathrm{PV,el,t\rightarrow U}} + E_{\mathrm{PG,el,t\rightarrow U}} + E_{\mathrm{BES,el,t\rightarrow U}} = \mathrm{E}_{\mathrm{U,el,t}} \quad (5)$$

$$E_{\mathrm{CHP,th,t\rightarrow U}} + E_{\mathrm{GB,th,t\rightarrow U}} + E_{\mathrm{TES,th,t\rightarrow U}} + E_{\mathrm{ASHP,th,t\rightarrow U}} + E_{\mathrm{STC,th,t\rightarrow U}} = E_{\mathrm{U,th,t}} \quad (6)$$

$$E_{\mathrm{CC,cool,t\rightarrow U}} + E_{\mathrm{AC,cool,t\rightarrow U}} + E_{\mathrm{ASHP,cool,t\rightarrow U}} = E_{\mathrm{U,cool,t}} \quad (7)$$

Equations (8)–(10) describe the energy exchange from PV and CHP systems to other MES components. In Equation (11), $E_{\mathrm{fuel\rightarrow CHP}}$ is the fuel energy (natural gas or H_2) input to the CHP system. In Equation (12), $E_{\mathrm{fuel\rightarrow GB}}$ plays the same role for a GB. Equation (13) imposes that CHP energy production complies with a high-efficiency co-generation constraint with an efficiency value set by EU legislation, which is 0.75 or 0.80 as a function of CHP technology [25].

$$E_{\mathrm{PV,el,t\rightarrow U}} + E_{\mathrm{PV,el,t\rightarrow PG}} + E_{\mathrm{PV,el,t\rightarrow BES}} + E_{\mathrm{PV,el,t\rightarrow CC}} + E_{\mathrm{PV,el,t\rightarrow ASHP}} = E_{\mathrm{PV,el,t}} \quad (8)$$

$$E_{\mathrm{CHP,el,t\rightarrow U}} + E_{\mathrm{CHP,el,t\rightarrow PG}} + E_{\mathrm{CHP,el,t\rightarrow ASHP}} + E_{\mathrm{CHP,el,t\rightarrow CC}} = E_{\mathrm{CHP,el,t}} \quad (9)$$

$$E_{\mathrm{CHP,th,t\rightarrow U}} + E_{\mathrm{CHP,th,t\rightarrow AC}} + E_{\mathrm{CHP,th,t\rightarrow TES}} = E_{\mathrm{CHP,th,t}} \quad (10)$$

$$E_{\mathrm{fuel\rightarrow CHP,t}} = \mathrm{LHV_{NG}}\, M_{\mathrm{NG\rightarrow CHP,t}} + \mathrm{LHV_{H2}}\, M_{\mathrm{H2\rightarrow CHP,t}} \quad (11)$$

$$E_{\mathrm{fuel\rightarrow GB,t}} = \mathrm{LHV_{NG}}\, M_{\mathrm{NG\rightarrow GB,t}} + \mathrm{LHV_{H2}}\, M_{\mathrm{H2\rightarrow GB,t}} \quad (12)$$

$$\sum_{\mathrm{t=1}}^{8760} E_{\mathrm{CHP,el,t}} + \sum_{\mathrm{t=1}}^{8760} E_{\mathrm{CHP,th,t}} \geq \eta_{\mathrm{HEC}} \sum_{\mathrm{t=1}}^{8760} E_{\mathrm{fuel\rightarrow CHP,t}} \quad (13)$$

CHP, STC and TES supply the thermal energy required by AC, as shown in Equation (14). According to Equations (15) and (16), both the ASHP and CC electrical energy demands are met by CHP, PV, BES and PG.

$$E_{\mathrm{AC,th,t}} = E_{\mathrm{CHP,th,t\rightarrow AC}} + E_{\mathrm{TES,th,t\rightarrow AC}} + E_{\mathrm{STC,th,t\rightarrow AC}} \quad (14)$$

$$\frac{E_{\mathrm{ASHP,th,t\rightarrow U}}}{\mathrm{COP_{ASHP}}} + \frac{E_{\mathrm{ASHP,cool,t\rightarrow U}}}{\mathrm{EER_{ASHP}}} = E_{\mathrm{CHP,el,t\rightarrow ASHP}} + E_{\mathrm{PV,el,t\rightarrow ASHP}} + E_{\mathrm{BES,el,t\rightarrow ASHP}} + E_{\mathrm{PG,el,t\rightarrow ASHP}} \quad (15)$$

$$\frac{E_{\mathrm{CC,cool,t\rightarrow U}}}{\mathrm{EER_{CC}}} = E_{\mathrm{CHP,el,t\rightarrow CC}} + E_{\mathrm{PV,el,t\rightarrow CC}} + E_{\mathrm{BES,el,t\rightarrow CC}} + E_{\mathrm{PG,el,t\rightarrow CC}} \quad (16)$$

Surplus electrical energy produced by PV is stored in the BES, of which the operation is managed by the binary variable Op_{BES}, which is equal to zero if PV charges the BES, and equal to 1 if the BES supplies electricity (see Equations (17) and (18)). These variables make the energy storage process asynchronous with respect to energy supply. Equation (19)

defines BES state of charge (*SoC*) on an hourly basis, by considering the self-discharge rate (SDR).

$$\frac{(E_{\mathrm{BES,el,t\rightarrow U}} + E_{\mathrm{BES,el,t\rightarrow ASHP}} + E_{\mathrm{BES,el,t\rightarrow CC}})}{\eta_{\mathrm{BES,disch}}} \leq Op_{\mathrm{BES}}\, E_{\mathrm{BES,max}} \tag{17}$$

$$E_{\mathrm{PVel\rightarrow BES}} \leq (1 - Op_{\mathrm{BES}})\ E_{\mathrm{PV,el}} \tag{18}$$

$$SoC_{\mathrm{BES,\,t}} = SoC_{\mathrm{BES,\,t-1}}\,(1 - \mathrm{SDR}) + E_{\mathrm{PV,el,t-1\rightarrow BES}}\,\eta_{\mathrm{BES}} - \frac{(E_{\mathrm{BES,el,t-1\rightarrow U}} + E_{\mathrm{BES,el,t-1\rightarrow CC}} + E_{\mathrm{BES,el,t-1\rightarrow ASHP}})}{\eta_{\mathrm{BES}}} \tag{19}$$

STC energy flows are managed by considering hot days (hd) and cold days (cd), according to Equations (20)–(23). The hot days are defined as the ones in which the daily average temperature is higher than 10 °C and the daily average irradiance is higher than 100 W/m^2. During hot days, STC can supply thermal energy to users, TES or AC (see Equation (20)). On the contrary, during cold days, STC can only charge TES. This operation is managed by the binary variable $Op_{\mathrm{STC,cd}}$. Instead, *isON* is a binary variable that indicates whether a system is switched on (1) or off (0). Therefore, if at least one between CHP, GB, or ASHP is turned on, STC can supply thermal energy to users or AC during cold days; on the contrary, if CHP, GB and ASHP are all switched off, STC can only charge TES. Equation (24) defines TES state of charge (SoC) on an hourly basis, where dc is the dissipation coefficient.

The optimal operation strategy identified by the MILP algorithm is assessed by evaluating the objective function expressed in Equation (4).

$$E^{\mathrm{hd}}_{\mathrm{STC_{th}\rightarrow u}} + E^{\mathrm{hd}}_{\mathrm{STC_{th}\rightarrow AC}} + E^{\mathrm{hd}}_{\mathrm{STC_{th}\rightarrow TES}} = E^{\mathrm{hd}}_{\mathrm{STC}} \tag{20}$$

$$E^{\mathrm{cd}}_{\mathrm{STC_{th}\rightarrow u}} + E^{\mathrm{cd}}_{\mathrm{STC_{th}\rightarrow AC}} = Op_{\mathrm{STC,cd}}\, E^{\mathrm{cd}}_{\mathrm{STC}} \tag{21}$$

$$E^{\mathrm{cd}}_{\mathrm{STC_{th}\rightarrow TES}} = \left(1 - Op_{\mathrm{STC,cd}}\right)\ E^{\mathrm{cd}}_{\mathrm{STC}} \tag{22}$$

$$Op_{\mathrm{cd,STC}} \leq isON_{\mathrm{CHP}} + isON_{\mathrm{GB}} + isON_{\mathrm{ASHP}} \tag{23}$$

$$SoC_{\mathrm{TES,\,t}} = SoC_{\mathrm{TES,\,t-1}}\,(1 - dc) + E_{\mathrm{CHP,th,t-1\rightarrow TES}} + E_{\mathrm{STC,th,t-1\rightarrow TES}} - E_{\mathrm{TES,th,t-1\rightarrow U}} - E_{\mathrm{TES,th,t-1\rightarrow AC}} \tag{24}$$

3. Energy Demand in the Hospital Sector

The yearly energy demand of a hospital building is estimated based on ref. [26], which reports the yearly values of electricity and thermal energy consumption during one year by fifty hospital buildings in the Piemonte region in Italy. The yearly primary energy consumption (due to both electrical and thermal energy) per unit floor area is split into five energy classes [27]:

1. Very high efficiency (primary energy consumption $\leq$ 250 kWh/m^2/year);
2. High efficiency (primary energy consumption from 250 kWh/m^2/year to 350 kWh/m^2/year);
3. Medium efficiency (primary energy consumption from 350 kWh/m^2/year to 500 kWh/m^2/year);
4. Low efficiency (primary energy consumption from 500 kWh/m^2/year to 600 kWh/m^2/year);
5. Very low efficiency (primary energy consumption $\geq$ 600 kWh/m^2/year).

Among the fifty hospital buildings considered in [26], in this study we consider hospitals with energy classes ranging from very high efficiency to high efficiency (i.e., primary energy consumption $\leq$ 350 kWh/m^2/year). In addition, we exclude hospitals that are equipped with CHP systems in order to evaluate actual hospital electrical and

thermal energy demands. As a result, twenty-one hospital buildings were selected to infer a correlation between energy consumption and floor area.

These twenty-one buildings are characterized by an average ratio between thermal and electrical energy consumption approximately equal to 1 and by degree day values ranging from 2500 to 3300. The "degree day" of a location refers to the sum, extended to all days of a conventional yearly heating period, of only the positive differences between the internal ambient temperature, conventionally set at 20 °C, and the average daily external ambient temperature [28].

As shown in Figure 2, two linear correlations, disclosed in Equations (25) and (26), are obtained to estimate the yearly electrical and thermal energy demand, expressed in [kWh/year], as functions of floor area, expressed in [m^2]. Both correlations have a coefficient of determination higher than 0.99. It is worth noting that Equation (25) provides the total electrical energy demand of the user by including both lighting and medical equipment, as well as the electricity consumed by CCs. Finally, electrical energy consumed by CC depends on the energy efficiency ratio (EER), as shown in Equation (27). Yearly thermal energy demand is calculated as in Equation (26), where $E_{U,th}$ accounts for the thermal energy required for both space heating and other uses, such as hot water and steam production.

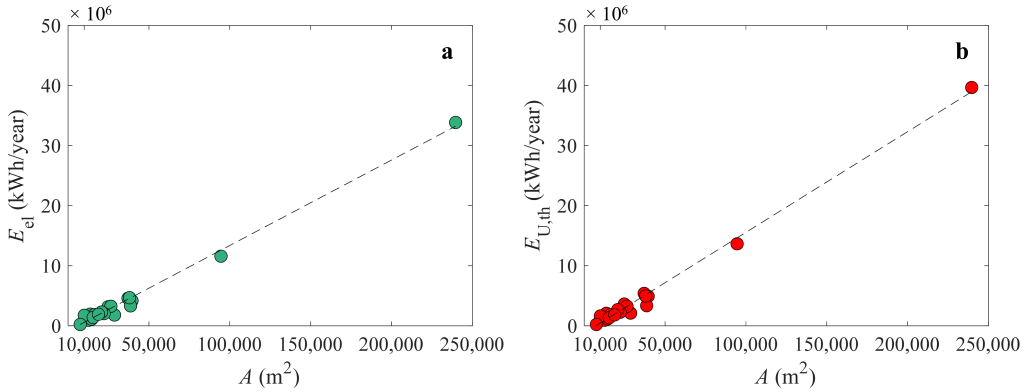


Figure 2. Electrical (**a**) and thermal (**b**) energy consumption as functions of hospital floor area.

The correlations reported in Equations (25) and (26) hold for the range of degree days specified above.

It must be noted that cooling energy demand ($E_{U,cool}$) is strongly influenced by the climatic zone and building typology [29], internal heat load, room location and orientation, as well as room usage and occupation data [5]. Study [30] demonstrated that hospitals display relatively limited sensitivity to climate change across different representative concentration pathways (RCPs) and climate zones.

$$E_{el} = E_{U,el} + E_{CC,el} = 142.21 \cdot A - 844,754 \quad (25)$$

$$E_{U,th} = 167.72 \cdot A - 1,212,167 \quad (26)$$

$$E_{CC,el} = \frac{E_{U,cool}}{EER_{CC}} \quad (27)$$

4. Case Study

The case study considered in this work is a hospital hypothetically located in the city of Torino, in northwestern Italy, of which energy demand data are consistent with the dataset presented in study [26]. The building has a floor area of 30,000 m^2, which is approximately the average floor area of the twenty-one hospitals used to derive the correlations developed

in the previous section. The total area suitable for PV and STC installation (i.e., A_{tot} in Appendix A), which accounts for the available rooftop area and parking lots, is 20,000 m^2.

The hourly non-dimensional profile of each energy demand is taken from study [31]. The yearly thermal and electrical energy demands are derived from Equations (25)–(27), which, as discussed in Section 3, were developed by using actual energy consumption. The yearly cooling energy demand is assumed on the basis of personal communications, while the EER of the compression chiller is assumed from manufacturers' catalogs (EER_{CC} = 4 represents a yearly average value [32]). In conclusion, the total yearly energy demands of the hospital located in Torino are $E_{U,el}$ = 2.92 GWh_{el}/year; $E_{U,th}$ = 3.82 GWh_{th}/year; $E_{U,cool}$ = 2.02 GWh_{cool}/year.

The procedure followed for estimating the 8760 h energy demands of the hospital is detailed below.

4.1. Energy Demands

The hourly thermal, electrical, and cooling energy demands over one year were derived from the non-dimensional profiles reported in [31]. In [31], the considered hospital was located in a city with an ambient temperature with a Pearson correlation coefficient higher than 0.93 with respect to the ambient temperature of the considered city (i.e., Torino, Italy). The data documents the ratio between the hourly energy demand and the yearly peak demand.

4.1.1. Thermal Energy Demand

For thermal energy demand, the non-dimensional profile of two typical days is available in [31]. The daily profile of one of the two days (red line in Figure 3(a.1)) accounts for the thermal energy required for both space heating ($E_{U,th,sp}$) and other uses ($E_{U,th,oth}$), such as hot water and steam production. The daily profile of the other day (orange line in Figure 3(a.1)) only includes $E_{U,th,oth}$, as the average monthly temperature is higher than a threshold (20 °C in this study) and thus the thermal energy demand for space heating is null.

In this work, $E_{U,th,oth}$ is assumed to be constant throughout the year, whereas space heating contribution ($E_{U,th,sp}$) is adjusted according to the average monthly temperature (T_{av}) by using the correction index *CI*, defined in Equation (28).

The coefficient *CI* is positive when the average monthly temperature is below 20 °C; otherwise, it is set to zero to cancel the contribution of space heating (see Figure 3(a.2)).

The average monthly temperature T_{av} is assumed to mimic a typical meteorological year and the data are derived from [33]. A typical meteorological year is a synthetic dataset representing the typical climate conditions of a specific location over one year. It is generated by selecting, month-by-month, the most representative meteorological data from a 19-year observation period (2005–2023), selecting the months that best match long-term average conditions while excluding extreme events such as heatwaves or cold spells [33,34].

Equation (29) is used to compute the hourly thermal energy demand for each month. February is the coldest month in Torino (Figure 3(a.2)) and thus exhibits the maximum thermal energy demand (Figure 3(a.3)), while the minimum demand occurs in June, July, and August.

The thermal energy demand is assumed to be identical for all days within a given month. Thus, the monthly non-dimensional energy demand is obtained by multiplying the daily demand by the number of days in the month. The yearly non-dimensional demand is the sum of the twelve monthly values.

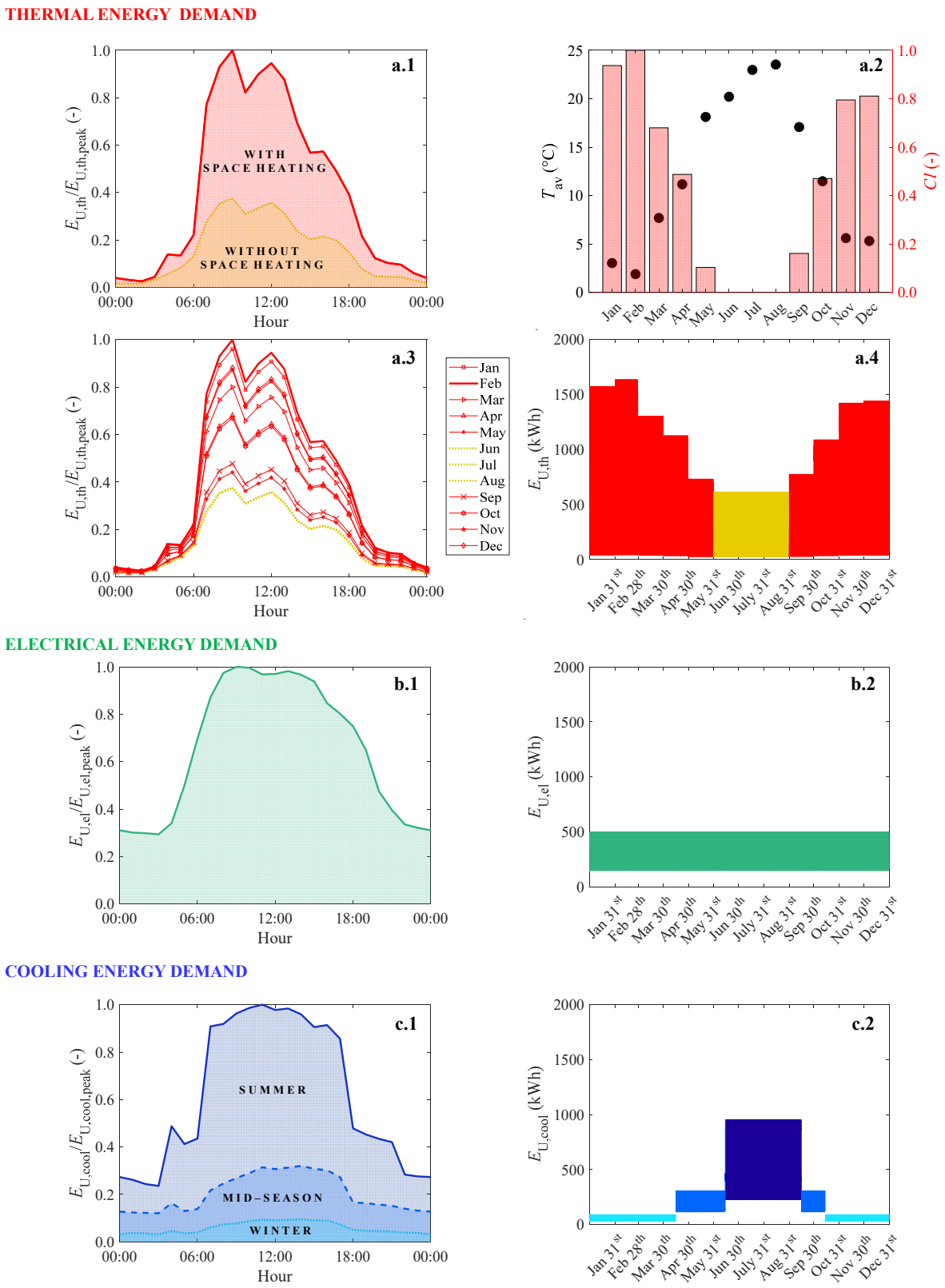


Figure 3. Procedure to derive hourly thermal (**a.1**–**a.4**), electrical (**b.1**,**b.2**), and cooling (**c.1**,**c.2**) energy demands.

Finally, the peak thermal energy demand is determined as the ratio of the yearly energy demand (i.e., 4.03 GWh/year for this case study) to the yearly non-dimensional demand. This peak value is used to scale the daily profiles in Figure 3(a.3). The replication

of these 24 h profiles throughout each day of the month provides the complete 8760 h profile illustrated Figure 3(a.4).

$$CI_{\mathrm{i}} = \frac{20 - T_{\mathrm{av,i}}}{20 - \min(T_{\mathrm{av}})} \tag{28}$$

$$E_{\mathrm{U,th}} = \left(E_{\mathrm{U,th,sp}} - E_{\mathrm{U,th,oth}}\right) \cdot CI + E_{\mathrm{U,th,oth}} \tag{29}$$

4.1.2. Electrical Energy Demand

For electrical energy demand, only one non-dimensional profile of a typical day is available in [31] (Figure 3(b.1)). Thus, this profile is applied to all 365 days, since user electricity demand (i.e., $E_{\mathrm{U,el}}$) remains nearly constant throughout the year, as it does not include CC consumption. Consequently, the total non-dimensional electricity demand over one year is obtained by multiplying the daily demand by 365 days. As with thermal energy demand, the peak value ($E_{\mathrm{U,el,peak}}$) is calculated as the ratio of yearly user electricity demand (i.e., 2.92 $\mathrm{GWh_{el}}$/year for this case study) to the yearly non-dimensional value. The hourly electricity demand is subsequently determined by multiplying the non-dimensional hourly profile (Figure 3(b.1)) by $E_{\mathrm{U,el,peak}}$; in each day, electrical energy demand ranges from 147 kWh to approximately 500 kWh. The hourly profile throughout one year is obtained by repeating this procedure, thus generating the full 8760 h electricity demand illustrated in Figure 3(b.2).

4.1.3. Cooling Energy Demand

For cooling energy demand, the non-dimensional profile of three typical days is available in [31], i.e., a winter day, mid-season day and summer day (Figure 3(c.1)). Cooling energy demand is assumed to be the same for all the days of a given season. Consequently, the non-dimensional seasonal energy demand is obtained by multiplying the daily demand by the number of days in the considered season, as reported below:

- 183 days in the winter season (i.e., 1st January–15th April and 15th October–31st December);
- 90 days in the mid-season (i.e., 16th April–14th June and 15th September–14th October);
- 92 days in summer (i.e., 15th June–14th September).

The total non-dimensional cooling energy demand for one year is calculated as the sum of the three seasonal values. As with the other variables, the peak cooling demand $E_{\mathrm{U,cool,peak}}$ is determined as the ratio of the yearly cooling energy demand (i.e., 2.02 GWh/year for the case study) to the corresponding non-dimensional value. The hourly cooling energy demand for each typical day is obtained by multiplying the corresponding non-dimensional hourly profile (Figure 3(c.1)) by $E_{\mathrm{U,cool,peak}}$. Once again, the 24 h dimensional profile of cooling energy demand throughout each day of a season can be inferred and is shown in Figure 3(c.2).

4.2. Energy and Economic Scenarios

In 2023, hospital energy demand was covered by the conventional plant (CP) shown in Figure 4, of which the configuration is fixed, and GB and CHP were fueled by natural gas. Instead, MES configuration in 2030 and 2050 can be optimized by means of the framework presented in Section 2. Such optimization identifies (i) the optimal size of all technologies shown in Figure 4, and (ii) the optimal operation of each technology hour-by-hour. In 2030, the conventional plant can be upgraded by integrating brand-new energy conversion and storage systems (i.e., ASHP, PV, STC, TES and BES). As in 2023, both GB and CHP are fueled by natural gas. Instead, in 2050, the MES is re-sized from scratch, and hydrogen is the only exploitable fuel. PSO hyperparameters are reported in Appendix A.

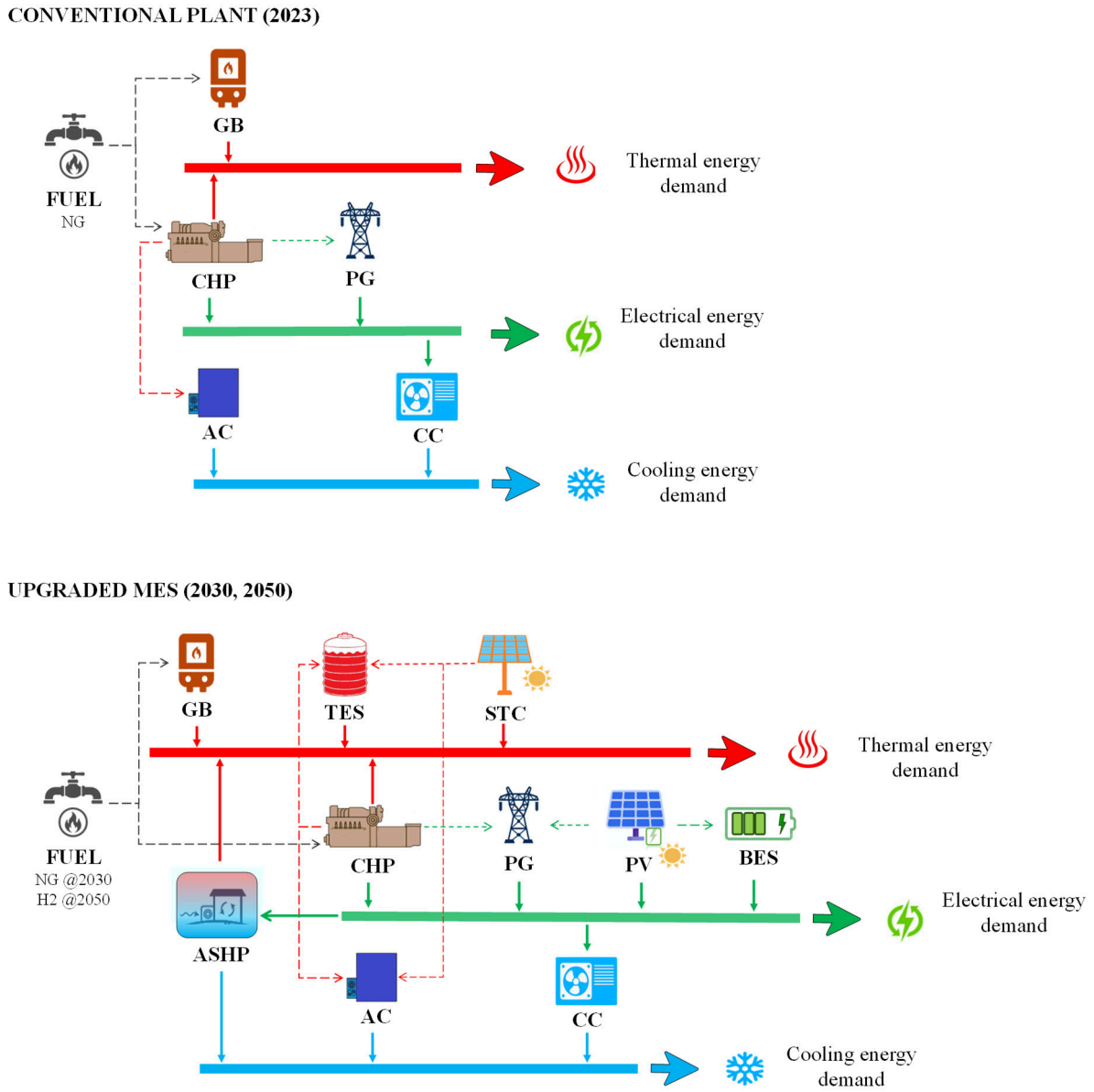


Figure 4. Technologies available for both conventional plant and upgraded MES.

It must be noted that power outages, equipment failures, reserve capacity, and N-1 security are not explicitly accounted for. However, given the need to assure reliable and uninterrupted energy supply, electrical, thermal, and cooling energy demand must be met at each time step, as discussed in Section 2.1.

Figure 5 shows the time evolution of energy prices, fuel costs, and CO_2 emission costs. Electricity and natural gas prices include taxes, as well as network and distribution costs associated with the Italian energy market [35–37]. Figure 5 reports the yearly average electricity price, but the annual cash flow is calculated by assuming that the electricity price varies on an hourly basis based on the three Italian time-of-use tariffs:

- T1 (Monday to Friday, from 8:00 a.m. to 7:00 p.m., excluding national holidays);
- T2 (Monday to Friday, from 7:00 a.m. to 8:00 a.m. and from 7:00 p.m. to 11:00 p.m., excluding national holidays; Saturdays, from 7:00 a.m. to 11:00 p.m., excluding national holidays):
- T3 (Monday to Saturday, from 12:00 a.m. to 7:00 a.m. and from 11:00 p.m. to 12:00 a.m.; Sundays and national holidays).

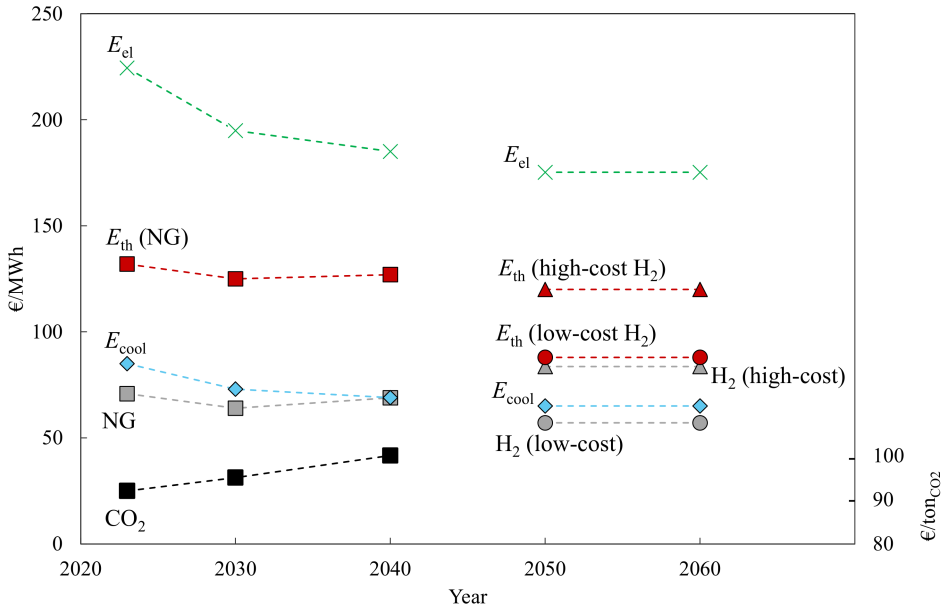


Figure 5. Electrical, thermal, and cooling energy price, NG cost, H2 cost and, CO_2 cost (tax-inclusive values) [35–37].

The electricity price for each time-of-use tariff until 2023 was derived from [35], whereas values until 2050 were projected based on the expected penetration of solar energy in the Italian electricity mix, starting from the historical values (Figure 6).

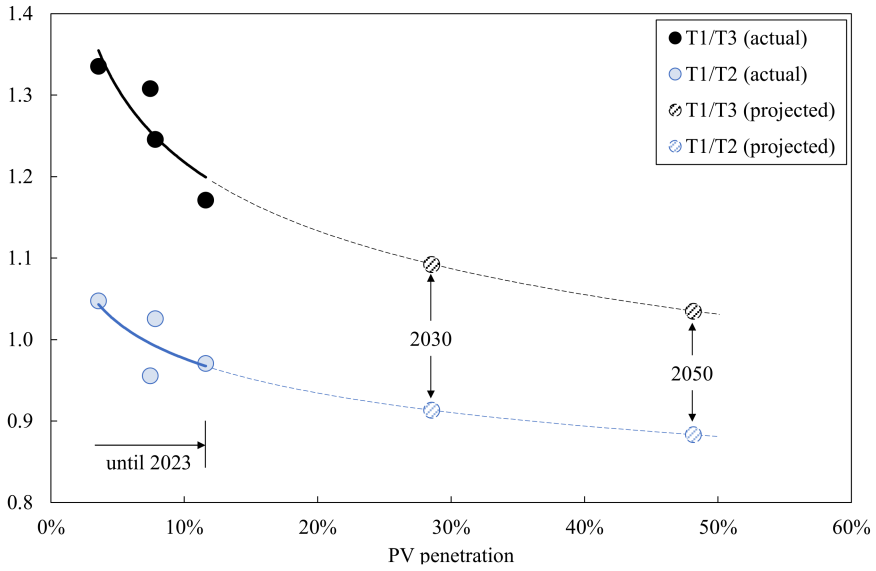


Figure 6. Ratio of time-of-use tariffs vs. PV penetration in Italy (solid line: actual value; dash line: projected value) [34,35].

4.2.1. Year 2023

The conventional plant includes gas boilers (GBs), sized to cover at least the thermal energy demand peak, compressor chillers (CCs) sized to cover at least the cooling energy demand peak, and a combined heat and power system (CHP), which in this study is assumed to be based on internal combustion engine technology, coupled with an absorption chiller (AC) to meet electrical, thermal and cooling energy demands, sized to maximize NPV (evaluated with a *ty* of 10 years and a DR of 5% [38]). The sizes of CP components are listed below:

- $Pth_{,des,GB}$ = 1637 kW_{th};

- $P_{cool,des,CC}$ = 1098 kW_{cool};
- $Pth_{,des,CHP}$ = 531 kW_{th};
- $P_{el,des,CHP}$ = 398 kW_{cool};
- $Pth_{,des,AC}$ = 531 kW_{th};
- $P_{cool,des,AC}$ = 399 kW_{cool}.

In addition, the power grid can be exploited to buy or sell surplus power generation.

The optimal operation of each CP component that maximizes profitability depends on energy prices, fuel cost and CO_2 emission cost shown in Figure 5. In this scenario, CHP and the power grid meet electrical energy demand by providing approximately 60% and 40% of the required energy respectively. CHP and GB also meet thermal energy demand by providing 60% and 40%, respectively. Cooling energy demand is met by CC in the order of 95%; the remaining share is supplied by AC.

Thermal energy price is indexed to natural gas (NG) cost. For this purpose, the specific revenue r_{Eth} (Equation (30)) is calculated by assuming that the total thermal energy demand is met by GB. Instead, the cooling energy demand is indexed to the electricity price; thus, the specific revenue r_{Ecool} (Equation (31)) is calculated by assuming that the total cooling energy demand is met by CC. The specific revenues (r_{Eth} and r_{Ecool}) are then multiplied by the corresponding energy demands to estimate the revenues $R_{Eth,sold}$ and $R_{Ecool,sold}$ obtained by selling thermal and cooling energy to the hospital.

$$r_{E_{th}} = \frac{AIn_{GB} + OPEX_{GB} + C_{NG,GB} + C_{CO2,GB}}{E_{GB,th \to U}} \quad (30)$$

$$r_{E_{cool}} = \frac{AIn_{CC} + OPEX_{CC} + C_{E_{el,CC}}}{E_{CC,cool \to U}} \quad (31)$$

4.2.2. Year 2030

In 2030, the CP components remain unchanged, as they consist of up-to-date technologies. The framework presented in Section 2 is used to evaluate whether the MES can be upgraded to incorporate new technologies among the ones included in Figure 4. In this scenario, the CAPEX in Equation (1) accounts for the capital cost of new technologies; the ACF in Equation (2) is evaluated as the difference between the ACF related to the optimized MES management strategy by considering the new configuration and the ACF corresponding to CP management strategy. This allows the evaluation of the possible benefit of employing additional technologies. The NPV of Equation (1) is evaluated for a time period ty of 10 years (namely, from 2030 to 2039) and a DR of 5% [38].

Thermal energy price is indexed to natural gas, while cooling energy price is indexed to the electricity price, as described above. As shown in Figure 5, natural gas and CO_2 costs are expected to increase over the time frame in order to discourage fossil fuel use. Consequently, the cost of thermal energy is also projected to rise. In contrast, the price of electricity is expected to slightly decrease.

4.2.3. Year 2050

In 2050, the entire MES is sized from scratch. Thus, CAPEX accounts for the capital cost of all new components. In this scenario, both GB and CHP are only fueled by H_2 [39–41], since it is assumed that an H_2 distribution network will be available in northwestern Italy in 2050 [42,43]. Therefore, thermal energy price is indexed to H_2, as reported in Equation (32). Additionally, CO_2 cost is not accounted for, as fossil fuels will be abandoned.

$$r_{E_{th}} = \frac{AIn_{GB} + OPEX_{GB} + C_{H2,GB}}{E_{GB,th \to U}} \quad (32)$$

Cooling energy price is indexed to the electricity price, according to Equation (31).

Over the 10-year time horizon (2050–2059), the DR is set at 5%. Energy prices and hydrogen costs are assumed to remain constant throughout the decade, as they are long-term forecasts of representative average values.

Two H_2 cost scenarios are considered—58 €/MWh and 84 €/MWh—referred to in this paper as "low-cost H2" and "high-cost H2", respectively. These H_2 costs include taxes, as well as hydrogen production and transportation costs [44]. As previously observed, electricity exhibits the highest cost, whereas cooling energy is the cheapest (Figure 5).

Table 1 summarizes the main technical specifications of MES components at design condition for the European Union. CAPEX, as well as OPEX (both fixed and variable components) are reported in Table 2. Each equation is specified by different parameters *k*, which depend on the considered scenario (Table 3).

Table 1. Technical specifications of MES components at design condition [15,32].

	Design Value		
Component	**2023**	**2030**	**2050**
CHP	$P_{th,des} = 3.027 \times P_{el,des}^{0.863}$		
	$\eta_{el,des} = 0.251 \times P_{el,des}^{0.073}$		
	$P_{el,des}$ and $Pth_{,des}$ are expressed in [kW]		
GB	$\eta_{th,des}$ = 0.93		
CC	EER = 5	EER = 5	EER = 6
AC	EER = 0.75		
ASHP		COP = 4.5	COP = 5.5
		EER = 4.5	EER = 5.5
PV	η_M = 0.20; η_{BoS} = 0.75		
STC	η_o = 0.8		
TES	*dc* = 0.5%		
BES	SDR = 0.02%		

Table 2. CAPEX and OPEX (fixed and variable components).

Component	u.o.m.	CAPEX (M€)	OPEX (k€/Year) (Fixed Component)	OPEX (€) (Variable Component)	Ref.
CHP	$P_{el,des}$ (MW_{el}) $E_{CHP_{el}}$ (MWh)	$k_{CHP,I} \cdot P_{el,des}{}^{-0.3} \cdot P_{el,des}$	$k_{CHP,FC} \cdot P_{el,des}$	$k_{CHP,VC} \cdot E_{CHP_{el}}$	[45]
GB	$Pth_{,des}$ (MW_{th}) $E_{GB,th}$ (MWh)	$k_{GB,I} \cdot P_{th,des}{}^{-0.15} \cdot P_{th,des}$	$k_{GB,FC} \cdot P_{th,des}$	$k_{GB,VC} \cdot E_{GB,th}$	[45]
CC	$P_{cool,des}$ (MW_{cool}) $E_{CC_{cool}}$ (MWh)	$k_{CC,I} \cdot 0.352 \cdot P_{cool,des}{}^{-0.122} \cdot P_{cool,des}$	$k_{CC,FC} \cdot P_{cool,des}$	$k_{CC,VC} \cdot E_{CC_{cool}}$	[45]
AC	$Pth_{,des}$ (MW_{th}) $E_{AC_{th}}$ (MWh)	$k_{AC,I} \cdot P_{th,des}{}^{-0.205} \cdot P_{th,des}$	$k_{AC,FC} \cdot P_{th,des}$	$k_{AC,VC} \cdot E_{AC_{th}}$	[40]
ASHP	$Pth_{,des}$ (MW_{th}) $E_{ASHP_{th}}$ (MWh) $E_{ASHP_{cool}}$ (MWh)	$k_{ASHP,I} \cdot 0.352 \cdot P_{th,des}{}^{-0.122} \cdot P_{th,des}$	$k_{ASHP,FC} \cdot P_{th,des}$	$k_{ASHP,VC} \cdot (E_{ASHP_{th}} + E_{ASHP_{cool}})$	[45]
PV	$P_{el,des}$ (MW_{el}) $E_{PV_{el}}$ (MWh)	$k_{PV,I} \cdot P_{el,des}$	-	$k_{PV,VC} \cdot E_{PV_{el}}$	[37]
STC	A (m^2)	$k_{STC,I} \cdot 2035\ (A)^{-0.15} \cdot A \cdot 10^{-6}$	$k_{STC,FC} \cdot A$	-	[45]
TES	$Eth_{,max}$ (MWh)	$k_{TES,I} \cdot E_{th,max}$	$k_{TES,FC} \cdot E_{th,max}$	-	[45,46]
BES	$E_{el,max}$ (MWh)	$k_{BES,I} \cdot E_{el,max}$	$k_{BES,FC} \cdot E_{el,max}$	$k_{BES,VC} \cdot E_{el \rightarrow BES}$	[47]

Table 3. Parameters for CAPEX and OPEX (fixed and variable components).

	CAPEX (k_I)			OPEX (Fixed Component k_{FC})			OPEX (Variable Component k_{VC})			
Component	**2023**	**2030**	**2050**	**2023**	**2030**	**2050**	**2023**	**2030**	**2050**	**Ref.**
CHP	1.11	0.8	0.8	9	9	9	7	7	7	[45]
GB	0.17	0.17	0.17	3	3	3	0.5	0.5	0.5	[45]
CC	1.12	0.97	0.88	3	2.7	2	1.8	1.7	1.6	[45]
AC	1.00	0.94	0.86	2	2	2	0.28	0.25	0.23	[45]
ASHP	2	1.74	1.57	3	2.7	2	1.8	1.7	1.6	[45]
PV	0.690	0.414	0.303	-	-	-	10	10	10	[37]
STC	1.00	0.90	0.77	2.3	2.1	1.4	-	-	-	[45]
TES	0.011	0.011	0.011	0.05	0.05	0.05	-	-	-	[45,46]
BES	0.386	0.267	0.267	0.95	0.78	0.78	0.5	0.5	0.5	[47]

5. Results and Discussion

This section reports the results of the optimal sizing and operation of the MES for the years 2023 and 2050. The sensitivity analyses are aimed at identifying the energy conversion technologies and storage systems that are expected to play a leading role in the hospital sector up to 2050, while accounting for uncertainty in electricity and fuel prices. For all scenarios, MES profitability is assessed by means of net present value, annual cash flow, discounted return on investment (DROI), discounted payback period (DPBP), and internal rate of return (IRR). DROI is calculated as in [48], while DPBP and IRR as in [49].

5.1. Year 2030

For the 2030 scenario, three analyses are conducted. First, the MES upgrade is performed by using the cost projections reported in Figure 5 (see "Baseline" sub-section). Then, profitability robustness is evaluated by varying natural gas and electricity prices. In the sub-section "Sensitivity analysis on MES operation", for the same upgraded MES configuration identified for the baseline scenario, operation is re-optimized by investigating eight additional combinations of natural gas and electricity costs. In the sub-section "Sensitivity analysis on MES sizing and operation", the upgraded MES is also re-sized from scratch (with the exception of CP components), and its operation is optimized accordingly by investigating two combinations of natural gas and electricity costs. In the following, Scenario A assumes a 25% increase in natural gas price compared to the Baseline scenario, combined with a 25% decrease in electricity price. Conversely, Scenario B considers a 25% increase in electricity price and a 25% decrease in natural gas price.

Baseline: The results of this analysis are quantitatively documented in Table 4 and Figures 7 and 8. An MES upgrade is evaluated in order to integrate new energy conversion and storage technologies (i.e., ASHP, PV, STC, TES, BES) into the conventional plant (whose size remains fixed). As shown in Table 4 (see column "Baseline"), the optimal upgraded MES includes all possible conversion and storage systems, with the exception of solar thermal collectors that are less competitive than photovoltaic panels.

The upgraded MES configuration is aimed to promote electrification of energy demand, reduce fossil fuel consumption, integrate energy storage technologies, and increase self-production. Electrification emerges from the predominance of photovoltaic panels, heat pumps, compression chillers in meeting energy demands. An interesting finding that can be drawn from the results is that cooling energy demand is entirely supplied by the compression chiller (see Figure 7), and heat pumps are preferably used only to meet thermal energy demand. In fact, cooling production with absorption chillers depends on two conversion efficiencies (i.e., $\eta_{th,CHP}$ and EER_{AC}) and accounts for CO_2 emissions from

CHP operation; in addition, EER_{CC} is higher than EER_{ASHP} (Table 1). In this scenario, energy storage systems are key components, especially TES that stores the surplus thermal energy produced by the CHP system, since the absorption chiller is not used (see Figure 7). Therefore, the use of GB and CHP systems may become more limited than in 2023 due to the increase in natural gas and CO_2 emission costs.

Table 4. Size of MES components in year 2030.

Components	Scenario A	Baseline	Scenario B
ASHP [kW_{th}]	633	547	172
ASHP [kW_{cool}]	1125	972	307
PV [m^2]	20,000	20,000	20,000
STC [m^2]	0	0	0
TES [m^3]	0	51	69
TES [kWh]	0	2917	3942
BES [kWh]	0	5.45	1.30

Finally, the upgraded MES enhances self-production, with most of the electricity demand supplied by PV and CHP systems. Approximately half of the electricity produced by PV is sold to the power grid, representing the primary revenue (see the Baseline bars in Figure 7). Consequently, only a limited share of electricity is purchased from the grid, resulting in relatively low expenditures, comparable in magnitude to CO_2-related and OPEX costs (Figure 7). As a result, ACF is positive, averaging 0.6 M€ per year. Accordingly, the MES upgrade proves economically viable, with positive values for both NPV and DROI (see the Baseline circles in Figure 8). In this scenario, the initial investment is recovered after approximately three and a half years (Figure 8c). Therefore, the proposed MES can be considered economically feasible.

Sensitivity analysis on MES operation: The sensitivity analysis on MES operation is carried out by analyzing eight additional cost combinations, in which electricity and natural gas prices are varied ±25% with respect to the Baseline scenario.

Under the considered projections, the results of the sensitivity analysis (see Figure 8) reveal that the upgraded MES is always economically more advantageous than the conventional plant, as DROI is always positive, independently of the price combinations. However, the profitability of the upgraded MES is strongly affected by electricity price: the higher the price, the higher the profitability. Indeed, if the natural gas price is fixed, NPV varies up to 60% if the electricity cost drops by 25%. Conversely, the natural gas price has only a marginal effect on profitability: in fact, if the electricity price is fixed, NPV changes by 5% at maximum if the natural gas price increases by 25%. Finally, the IRR and DROI exhibit a similar trend. Across all the analyzed scenarios, the initial investment is recovered within a maximum of four years. This payback period is less than half the assumed MES lifetime, further supporting the economic feasibility of the proposed solution.

The sensitivity analysis therefore shows that the optimization framework allows us to identify the optimal operation strategy that makes the investment always profitable and robust under varying economic scenarios.

Sensitivity analysis on MES sizing and operation: In this section, both the sizes of the newly integrated technologies (i.e., ASHP, PV, STC, TES, and BES) and the overall MES operation are optimized from scratch to assess the influence of variations in electricity and natural gas prices on MES profitability. The outcomes for the Baseline scenario as well as Scenarios A and B are shown and compared in Table 4 and Figures 7 and 9.

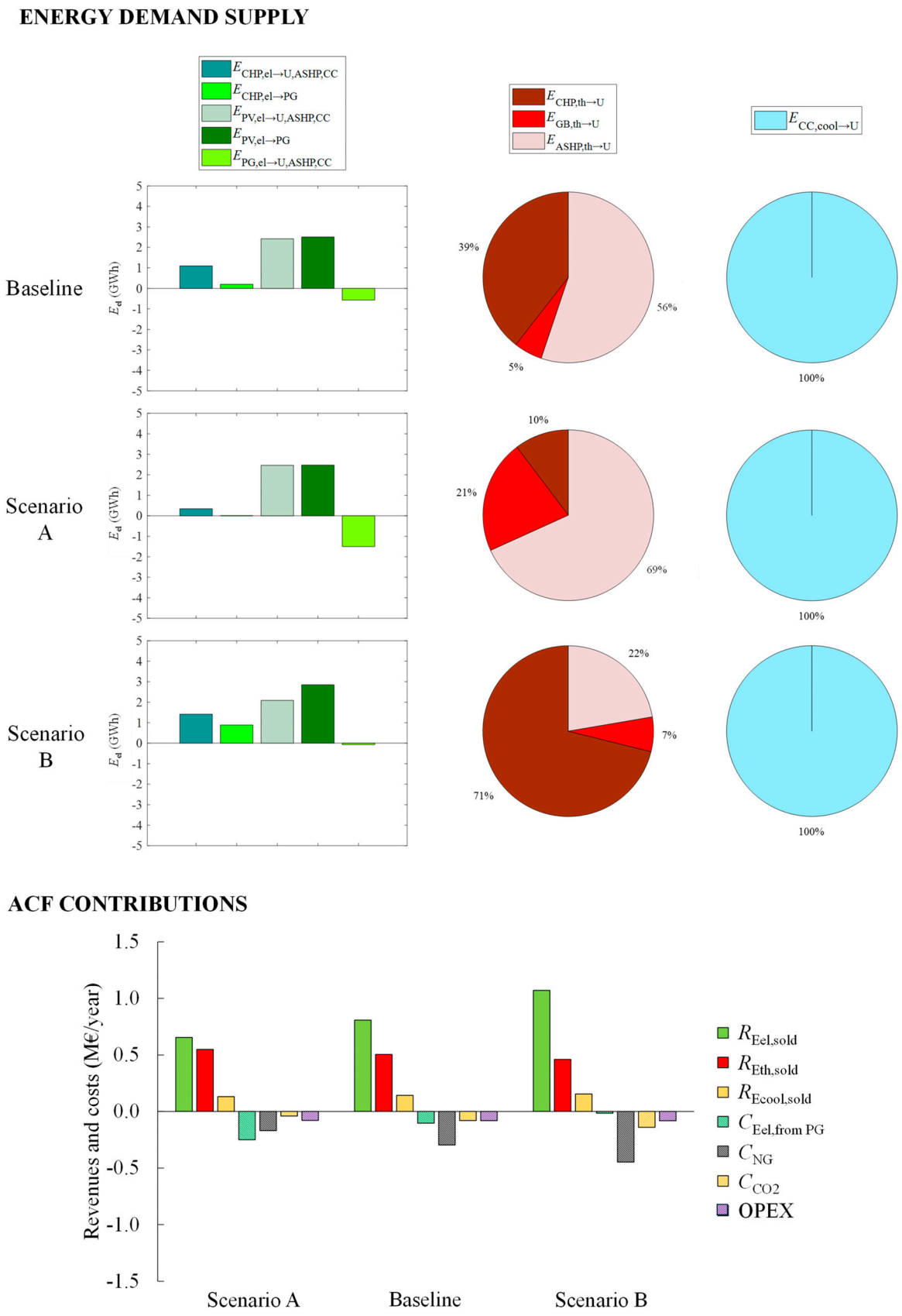


Figure 7. Results of the sensitivity analysis on MES sizing and operation (2030).

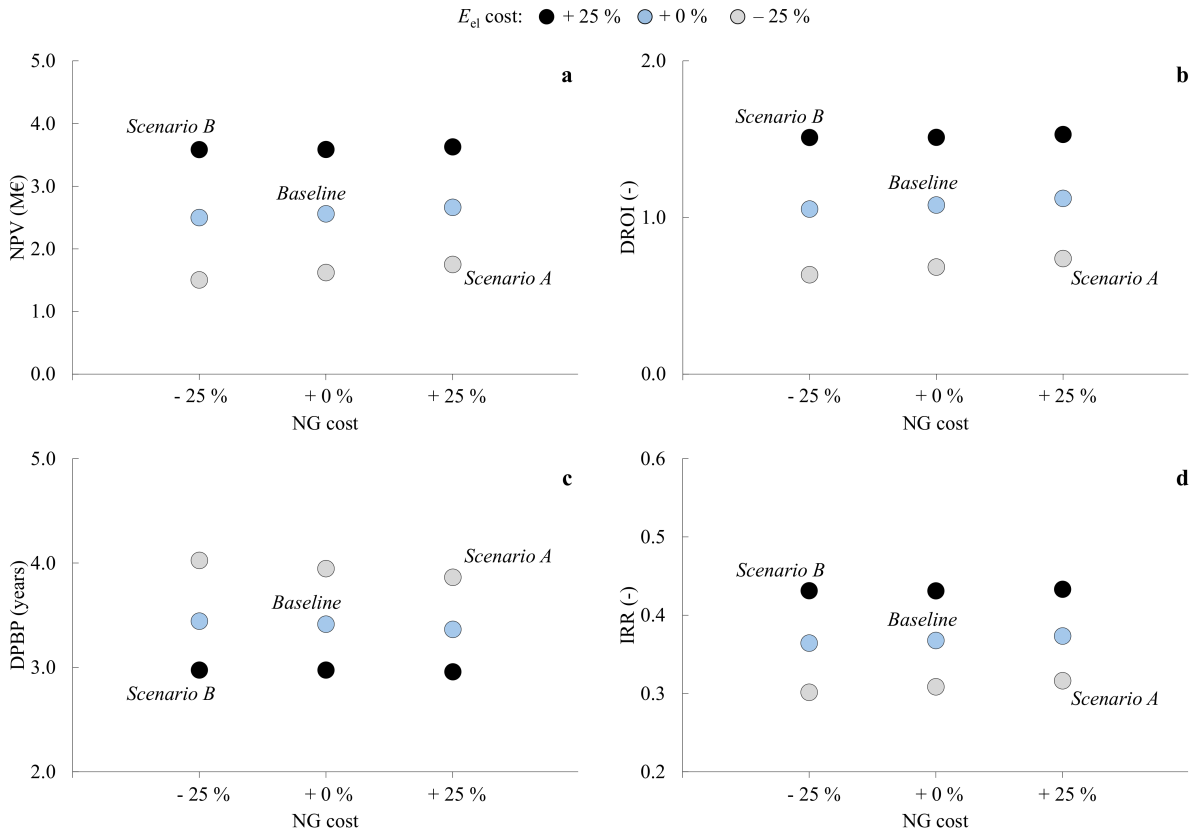


Figure 8. NPV (**a**), DROI (**b**), DPBP (**c**), and IRR (**d**) values for 2030 (sensitivity analysis on MES operation).

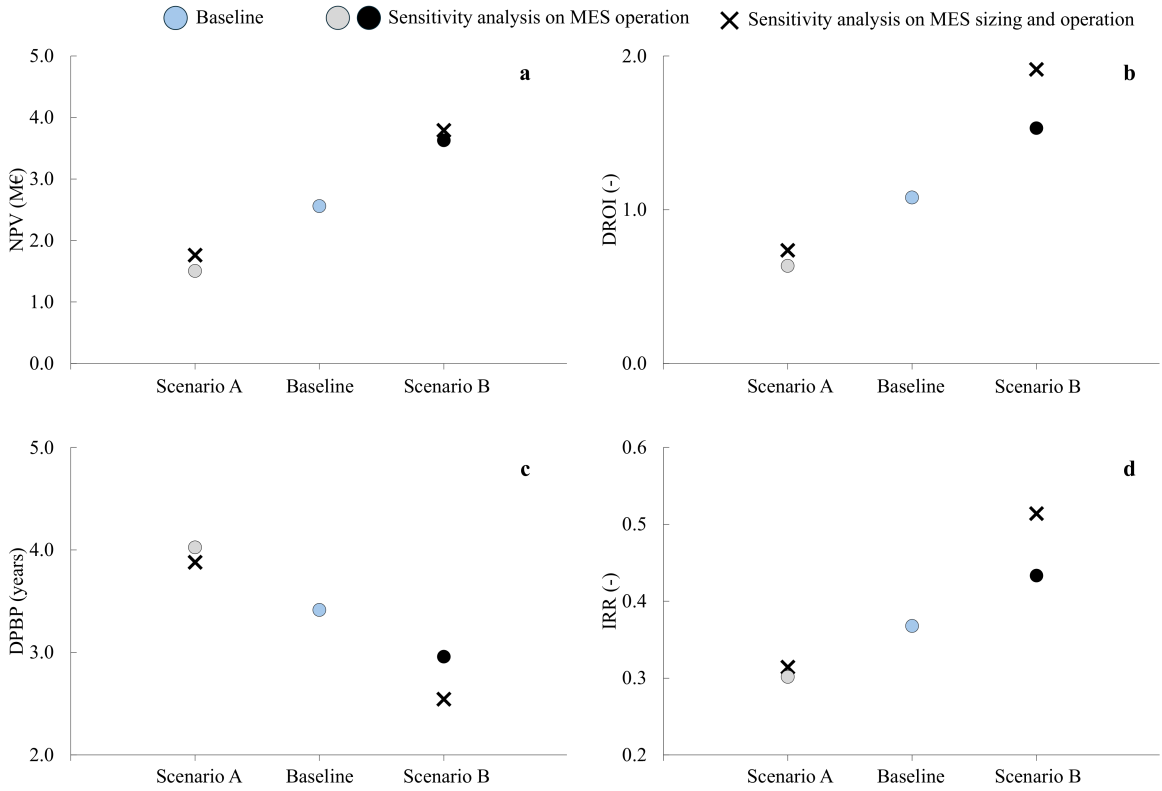


Figure 9. Comparison of NPV (**a**), DROI (**b**), DPBP (**c**), and IRR (**d**) in 2030.

In Scenario A, as expected, the increase in natural gas price combined with a reduction in electricity cost further promotes electrification of energy demands and leads to a decrease

in fuel consumption. Consequently, PV panels are highly profitable, since their installation is recommended on the entire available area (Table 4). Since this outcome is also observed in the Baseline scenario, the contribution of PV systems to meet electricity demand remains approximately unchanged (Figure 7). The attractiveness of heat pumps further increases, by satisfying most of the thermal energy demand (i.e., 69%) at the expense of fossil-fuel-based technologies (i.e., GB and CHP). The contribution of the CHP system also significantly drops in meeting electricity demand. In fact, under the considered projections, purchasing electricity from the power grid becomes economically preferable—thanks to its lower cost—compared to on-site generation. As a result, the integration of energy storage systems (both TES and BES) is strongly discouraged, and overall self-production decreases. From an economic perspective, the investment in upgrading the MES remains profitable, as DROI is positive (see black cross in Figure 9); however, it is less economically attractive than the configuration obtained in the Baseline scenario. In fact, NPV, DROI, and IRR decrease, while DPBP increases. Based on the sensitivity analysis documented in Figure 8, this finding can be mainly attributed to the decrease in electricity price.

In Scenario B, the decrease in natural gas price combined with the increase in electricity cost has a clear impact on CHP operation, which now meets the majority of the thermal energy demand (approximately 71%) as well as a significant share of the user electricity demand. As a result, heat pumps appear less competitive. Also in this case, photovoltaic panels occupy the entire available area. Consequently, all surplus electricity generation (from both CHP and PV) is sold to the PG, whereas electricity purchased from the PG is negligible. Therefore, this scenario pushes fuel consumption, encourages the integration of energy storage systems (especially TES), and promotes self-production, whereas discourages electrification of energy demand.

In conclusion, the reduction in fuel cost combined with higher electricity prices maximizes the profitability of the upgraded MES, achieving the highest NPV (i.e., approximately 4 M€), DROI (i.e., approximately 1.9), and IRR (i.e., approximately 0.51), and minimum DPBP (i.e., approximately 2.5 years) across the three scenarios (see Figure 9).

Comparison: The main outcomes for Scenarios A and B of the two sensitivity analyses are compared in Figure 9. In Scenario A, the optimization framework preserves investment profitability regardless of cost variations. In fact, even if the MES is not optimally sized with respect to present costs (gray circle), an optimal operation strategy can yield comparable investment performance, making profitability largely independent of initial sizing. In contrast, in Scenario B, investment profitability is strongly affected by sizing choices. In fact, an optimally sized and managed MES (cross in Figure 9) achieves a 27% higher DROI than the baseline configuration where only operational management is optimized (black circle in Figure 9). This outcome indicates that optimal sizing becomes a decisive factor for overall investment performance when electricity price increases.

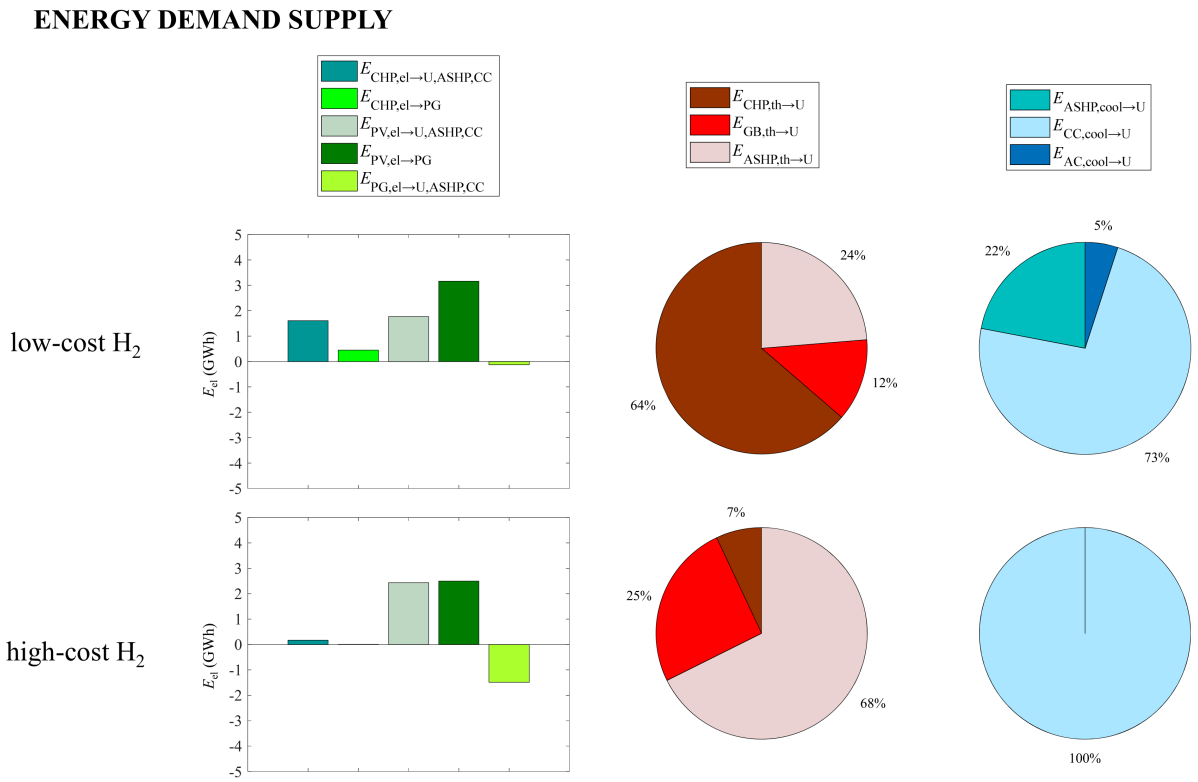
To sum up, these findings further highlight that an optimization tool for both sizing and operation is essential under uncertain and highly volatile economic conditions, especially when electricity prices are expected to vary, even dramatically. From an operational perspective, the framework enables decision-makers to rapidly identify the most suitable management strategy according to market conditions, thereby reducing investment risk while supporting the progressive electrification and decarbonization of the hospital sector.

5.2. 2050 Scenario

In 2050, the MES is sized from scratch, assuming that both the GB and CHP units are exclusively fueled by hydrogen. The optimal sizes are reported in Table 5, while the corresponding energy supply and ACF contributions are shown in Figure 10.

Table 5. Size of MES components in 2050 scenario.

Component	"Low-Cost H_2" Scenario	"High-Cost H_2" Scenario
CHP [kW_{el}]	307	42
CHP [kW_{th}]	425	76
GB [kW_{th}]	1430	1044
CC [kW_{cool}]	335	919
AC [kW_{th}]	252	0
AC [kW_{cool}]	189	0
ASHP [kW_{th}]	207	593
ASHP [kW_{cool}]	377	1078
PV [m^2]	20,000	20,000
STC [m^2]	0	0
TES [m^3]	89	11
TES [kWh]	5086	628
BES [kWh]	0	328



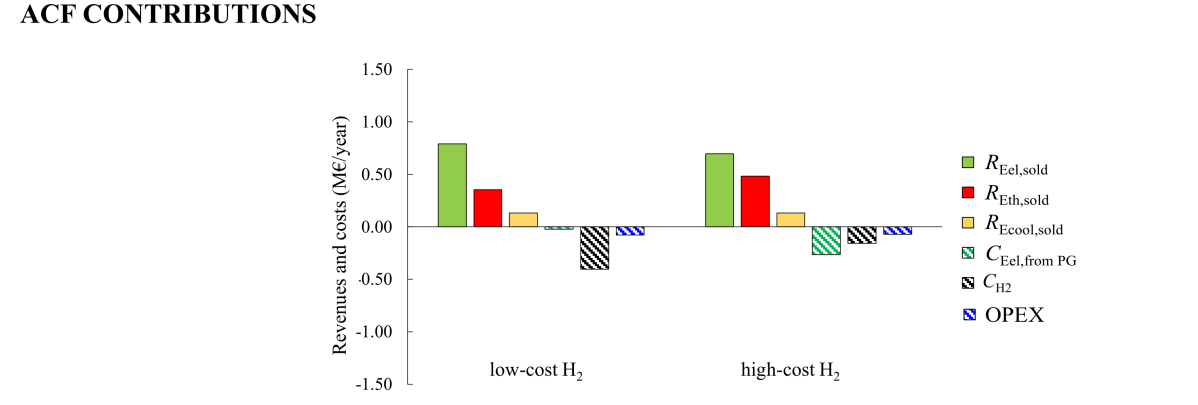


Figure 10. Results of the sensitivity analysis on MES sizing and operation (2050).

Independently of H_2 cost, the optimal size of all the technologies composing the conventional plant (i.e., boiler, gas boiler, compression chiller, and absorption chiller) decreases, but they are required to operate more frequently and at higher loads (see Figure 10). This finding especially applies to the "low-cost H_2" scenario, in which CHP size decreases by approximately 20%, but power production increases by more than 60% with respect to 2030. In addition, GB remains the heating source with the largest size. Nevertheless, its actual contribution is limited, confirming its role as a peak-load and backup technology rather than a primary heat source. As shown in Table 5, costs significantly affect the optimal sizing of each unit. An interesting result emerges about GB: the relative decrease in its optimal size is lower than the relative increase in hydrogen cost (see Table 5). By contrast, the impact of hydrogen cost fluctuations on the sizing of the heat pump—and especially the CHP unit—is considerably more pronounced. As a rule of thumb, an increase in H_2 cost reduces the level of MES self-sufficiency and accelerates the electrification of energy demand. In this scenario, purchasing electricity from the grid becomes more economically attractive than on-site generation through the CHP unit, while heat pumps increasingly dominate system operation. PV systems remain consistently attractive from both an energy and an economic perspective. Based on the assumed cost projections, solar thermal collectors do not reach competitiveness and are therefore excluded from all scenarios. The strategy for meeting cooling energy demand is affected by H_2 cost, although compressor chillers will continue to play a predominant role (Figure 10). Heat pumps, compression chillers, and absorption chillers will all be utilized, but only if hydrogen cost remains low. Only under this scenario are reversible heat pumps a potentially cost-effective option. In addition, the absorption chiller only contributes to about 5% of the total cooling energy demand and is primarily used to cover peak loads.

From an economic standpoint, MES remains viable under both hydrogen cost scenarios, exhibiting positive DROI values (blue circles in Figure 11). This outcome is primarily driven by the revenues from the sale of electricity generated by the PV systems and CHP unit (see Figure 10). Moreover, although hydrogen cost increases by approximately 45% when moving from the "low-cost H_2" scenario to the "high-cost H_2" scenario—leading to significant changes in the MES configuration—the overall profitability is only marginally affected. Specifically, NPV increases by 8%, DROI rises by 3% (blue circles in Figure 11), IRR increases by 2%, and DPBP reduces by 2%. As already highlighted in the comments about the 2030 scenario, the availability of the proposed optimization framework is essential to tackle cost variability while ensuring system's economic viability.

These results demonstrate that the proposed framework can effectively support strategic and operational decisions in long-term planning, allowing stakeholders to evaluate alternative technology pathways and adapt system operation to future energy market conditions. Such capability represents an important contribution towards the implementation of reliable and economically sustainable strategies in critical infrastructure such as hospitals in the context of energy transition.

Sensitivity analysis on MES operation: A sensitivity analysis was conducted by freezing the size of MES components (see Table 5) while its operation was optimized under different electricity prices (black and gray circles in Figure 11). This analysis shows that an increase in electricity price leads to higher NPV, DROI, and IRR values; as a result, the payback period reduces. In contrast, the MES proves to be more resilient to fuel price fluctuations: an increase in fuel cost (from "low-cost H_2" to "high-cost H_2") results in a smaller relative change in DROI.

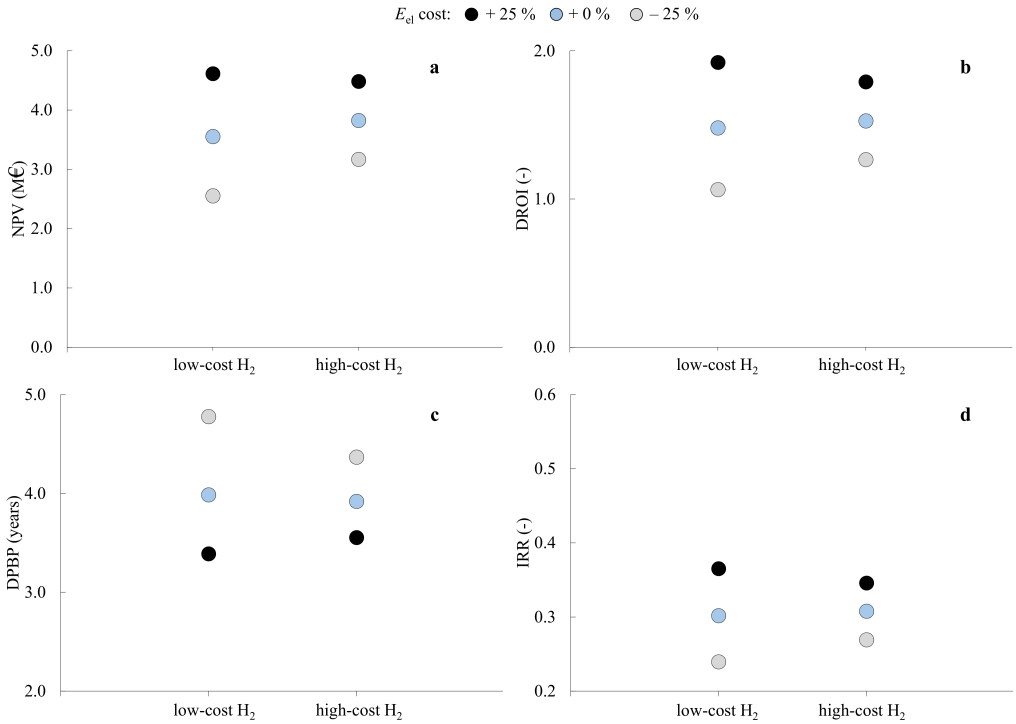


Figure 11. NPV (**a**), DROI (**b**), DPBP (**c**), and IRR (**d**) values for 2050 (sensitivity analysis on MES operation).

5.3. Key Findings

The analyses conducted for the 2030 and 2050 scenarios reveal some common directions, which are summarized and discussed below:

- From an economic standpoint, a MES composed of multiple energy conversion systems may be more viable than a conventional plant. Such an investment improves long-term profitability as both NPV and DROI values are usually higher in 2050 than in 2030. This result is consistent with the findings reported in [50], which demonstrated the limited economic attractiveness of gas-based self-generation.
- The variation in electricity cost is the dominant factor when assessing MES viability. In addition, the higher electricity price, the higher investment profitability. In contrast, the MES proves to be more resilient to fuel price fluctuations: an increase in fuel cost results in a smaller relative change in DROI. This result is consistent with the findings reported in [51], which demonstrated that electricity prices, along with peak sunlight hours and investment costs, are the main factors influencing system outcomes.
- In future years, the contribution of H_2-fueled CHP systems and gas boilers used to meet energy demands may be limited. Specifically, gas boilers may be expected to operate primarily as peak-load shavers. This result is consistent with the findings reported in [52], in which boilers were considered for peak heat demands.
- Photovoltaic panels will remain attractive from both an energy and an economic perspective. This result is consistent with the findings reported in [53], which showed that photovoltaic panel capacity has the greatest influence on both economic and environmental outcomes.
- The installation of solar thermal collectors and absorption chillers may be discouraged, as they are usually less competitive from both an energy and an economic standpoint compared to alternative technologies. This result is consistent with the findings reported in [54], which concluded that compression chillers are the best option for cooling systems with variable demand while absorption chillers are a good choice for systems with constant demand (e.g., data centers).

- Heat pumps may be more and more strategic when electricity price decreases, whereas CHP systems are preferable when fuel cost decreases. This result is consistent with the finding reported in [55], which demonstrated that CHP systems tend to lose competitiveness when electricity price reduces.
- In the investigated scenarios that consider a slightly lower EER_{ASHP} than EER_{CC}, reversible heat pumps are usually discouraged, as cooling energy demand will be largely met by compression chillers.
- The economic viability of thermal energy storage integrated with CHP systems is highly sensitive to fuel and electricity prices. TES can improve CHP economics by enabling surplus heat production to be stored and subsequently dispatched when economically advantageous. In contrast, batteries are generally less appealing energy- and economics-wise . These findings are consistent with [56], which stated that TES is the most utilized storage associated with CHP systems.

In summary, the framework developed in this paper proves to be a key tool for optimizing both the sizing and operation of a MES, mainly under uncertain and highly volatile economic conditions.

6. Conclusions

This study investigated the role of multi-generation energy systems (MESs) in hospital buildings for the years 2030 and 2050. To this end, an optimization framework was developed to concurrently optimize the sizing and operation of MESs, enabling the identification of the most feasible energy system configuration under different future energy scenarios.

The proposed optimization framework was applied to a hospital located in Torino (Italy) to investigate possible MES upgrade pathways for the target years 2030 and 2050. The analyses incorporated projected variations in energy prices, investment costs, technological performance, and the future availability of hydrogen distribution infrastructures.

The results highlighted electricity price as the most influential parameter affecting MES profitability. In particular, higher electricity prices significantly enhanced the economic viability of the proposed configurations, whereas MES profitability exhibited greater resilience to fuel price variations. Combined heat and power units remained strategic, especially under conditions of reduced hydrogen prices. Conversely, heat pumps became increasingly attractive in scenarios characterized by lower electricity costs.

Despite the variability among the analyzed scenarios, all optimized MES configurations yielded positive NPV and discounted return on investment (DROI) values, confirming the economic feasibility of the proposed solutions. Among the considered scenarios, the most favorable configuration was identified for the 2050 scenario, with NPV values reaching 4.6 M€ and DROI values up to 1.9. Finally, the discounted payback period was shorter than five years in all scenarios; this result indicates that the initial investment is recovered well before the end of the MES expected operational lifetime (i.e., 10 years).

Overall, the proposed optimization framework goes beyond the identification of optimal technology sizes by providing practical support for operational and investment decision-making. Its capability of jointly optimizing MES configuration and operation under different scenarios will enable stakeholders to evaluate robust transition pathways while accounting for uncertainties in energy prices and fuel costs. Therefore, the framework represents a valuable decision-support tool for planning the decarbonization of hospital energy systems and facilitating the broader energy transition towards more sustainable and resilient healthcare infrastructures.

Future works will investigate the impact of uncertainty on additional influential parameters (e.g., energy demand and investment costs) on the size and operation of MESs.

In addition, future studies will address the potential impacts of the MES on CO_2 emissions, emission reductions, and renewable energy penetration.

Author Contributions: Conceptualization, G.A.M.C., L.M., P.R.S. and M.V.; methodology, G.A.M.C., L.M., P.R.S. and M.V.; software, G.A.M.C.; validation, G.A.M.C., L.M., P.R.S. and M.V.; formal analysis, G.A.M.C., L.M., P.R.S. and M.V.; data curation, G.A.M.C., L.M., P.R.S. and M.V.; writing—original draft preparation, G.A.M.C., L.M., P.R.S. and M.V.; writing—review and editing, G.A.M.C., L.M., P.R.S. and M.V.; visualization, G.A.M.C., L.M., P.R.S. and M.V.; supervision, P.R.S. and M.V.; project administration, P.R.S.; funding acquisition, P.R.S. All authors have read and agreed to the published version of the manuscript.

Funding: This research was funded by (i) the EU—Next Generation EU, Mission 4, Component 1, CUP D53D23004440006, project title "Smart Energy in Cities and Communities for 2050" (Prot. 2022ZM87LR) and (ii) "PR-FESR EMILIA ROMAGNA 2021–2027", within the context of the "PIAC(ER)2" project—CUP E37G22000560007.

Data Availability Statement: The original contributions presented in the study are included in the article, further inquiries can be directed to the corresponding author.

Conflicts of Interest: The authors declare no conflicts of interest.

Nomenclature

A	area
c	specific heat capacity
C	cost
E	energy
k	parameter
M	mass
n	number
Op	operation
r	specific revenue
R	revenue
T	temperature
ty	time period (year)
η	efficiency
ρ	density
Subscripts and superscripts	
av	average
BOS	balance of systems
cd	cold day
cool	cooling
des	design
disch	discharge
el	electrical
hd	hot day
I	investment cost (CAPEX)
M	module
o	optical
oth	other uses
r	specific revenue
sp	space heating
t	time step
th	thermal
tot	total
U	user
Acronyms	
AIn	yearly installment
AC	absorption chiller
ACF	yearly cash flow
ASHP	air source heat pump

BES	battery energy storage
CAPEX	capital expenditure
CC	compression chiller
CHP	combined heat and power system
CI	correction index
COP	coefficient of performance
dc	dissipation coefficient
DR	discount rate
EER	energy efficiency ratio
FC	fixed component of OPEX
GB	gas boiler
H2	hydrogen
HEC	high-efficiency co-generation
LHV	lower heating value
MES	multi-generation energy system
MILP	mixed-integer linear programming
NG	natural gas
NPV	net present value
OPEX	operational expenditure
PG	power grid
PSO	particle swarm optimization
PV	photovoltaic panel
DROI	discounted return on investment
SDR	self-discharge rate
SoC	state of charge
STC	solar thermal collector
TES	thermal energy storage
VC	variable component of OPEX

Appendix A

Table A1. PSO algorithm settings and parameter constraints.

Hyperparameter	**Value**
Swarm size	50 (2030), 70 (2050)
Inertia weight strategy	Adaptive inertia strategy
Inertia range	[0.3, 1.2]
Cognitive coefficient	1.5
Social coefficient	1.5
Lower and upper bounds	**ASHP (2030, 2050)** $P\text{th}_{,\text{des}} \in [0, P\text{th}_{,\text{max,U}}]$ **TES (2030, 2050)** $E\text{th}_{,\text{max}} \in [0, \frac{\rho \cdot c \cdot \Delta T}{3600} \cdot \left\{ \frac{A_{\text{STC}} \cdot 60}{1000} + 10 \cdot \left[\frac{A_{\text{tot}} \cdot 60}{1000} + \frac{3600 \cdot 2 \cdot P_{\text{th,CHP,des}}}{\rho \cdot c \cdot \Delta T} \right] \right\}]$ where $\Delta T = 50$ °C [13] **BES (2030, 2050)** $E_{\text{el,max}} \in [0, 5 \cdot A_{\text{tot}} \cdot G_{\text{std}} \cdot \eta_{\text{M,rif}} \cdot \Delta t]$ where $G_{\text{std}} = 1000$ W/m^2 **STC (2030, 2050)** $A_{\text{STC}} \in [0, A_{\text{tot}} - A_{\text{PV}}]$ **PV (2030, 2050)** $A_{\text{PV}} \in [0, A_{\text{tot}}]$ **CC (2050)** $P_{\text{cool,des}} \in [0, P_{\text{cool,max,U}}]$ **CHP (2050)** $P_{\text{el,des}} \in [0, P_{\text{el,max,U}}]$
Start values	0.5·Upper bound
Function tolerance	10^{-6}
Max iterations	12
Max stall iteration	20
Computational platform	Matlab2025®

References

1. García-Sanz-Calcedo, J.; Gómez-Chaparro, M.; Sanchez-Barroso, G. Electrical and thermal energy in private hospitals: Consumption indicators focused on healthcare activity. *Sustain. Cities Soc.* **2019**, *47*, 101482. [CrossRef]
2. Shi, Y.; Yan, Z.; Li, C.; Li, C. Energy consumption and building layouts of public hospital buildings: A survey of 30 buildings in the cold region of China. *Sustain. Cities Soc.* **2021**, *74*, 103247. [CrossRef]
3. Chung, J.W.; Meltzer, D.O. Estimate of the carbon footprint of the US health care sector. *JAMA J. Am. Med. Assoc.* **2009**, *302*, 1970–1972. [CrossRef] [PubMed]
4. Greensmith, H.; Head, F.; Heidel, K.; Pencheon, D.; Roschnik, S.; Wrigh, S. NHS—Sustainable Development Unit. Available online: https://www.england.nhs.uk/greenernhs/whats-already-happening/sustainable-development-unit-archive/ (accessed on 3 March 2025).
5. Čongradac, V.; Prebiračević, B.; Jorgovanović, N.; Stanišić, D. Assessing the energy consumption for heating and cooling in hospitals. *Energy Build.* **2012**, *48*, 146–154. [CrossRef]
6. Eckelman, M.J.; Sherman, J. Environmental Impacts of the U.S. Health Care System and Effects on Public Health. *PLoS ONE* **2016**, *11*, e0157014. [CrossRef] [PubMed]
7. Christiansen, N.; Kaltschmitt, M.; Dzukowski, F. Electrical energy consumption and utilization time analysis of hospital departments and large scale medical equipment. *Energy Build.* **2016**, *131*, 172–183. [CrossRef]
8. García-Sanz-Calcedo, J. Analysis on Energy Efficiency in Healthcare Buildings. *J. Healthc. Eng.* **2014**, *5*, 361–374. [CrossRef] [PubMed]
9. Santamouris, M.; Dascalaki, E.; Balaras, C.; Argiriou, A.; Gaglia, A. Energy performance and energy conservation in health care buildings in hellas. *Energy Convers. Manag.* **1994**, *35*, 293–305. [CrossRef]
10. Capozzoli, A.; Piscitelli, M.S.; Gorrino, A.; Ballarini, I.; Corrado, V. Data analytics for occupancy pattern learning to reduce the energy consumption of HVAC systems in office buildings. *Sustain. Cities Soc.* **2017**, *35*, 191–208. [CrossRef]
11. Buonomano, A.; Calise, F.; Ferruzzi, G.; Palombo, A. Dynamic energy performance analysis: Case study for energy efficiency retrofits of hospital buildings. *Energy* **2014**, *78*, 555–572. [CrossRef]
12. García-Sanz-Calcedo, J.; Gómez-Chaparro, M. Quantitative analysis of the impact of maintenance management on the energy consumption of a hospital in Extremadura (Spain). *Sustain. Cities Soc.* **2017**, *30*, 217–222. [CrossRef]
13. Bahlawan, H.; Castorino, G.A.M.; Losi, E.; Manservigi, L.; Spina, P.R.; Venturini, M. Optimal management with demand response program for a multi-generation energy system. *Energy Convers. Manag. X* **2022**, *16*, 100311. [CrossRef]
14. Bahlawan, H.; Morini, M.; Pinelli, M.; Spina, P.R.; Venturini, M. Simultaneous optimization of the design and operation of multi-generation energy systems based on life cycle energy and economic assessment. *Energy Convers. Manag.* **2021**, *249*, 114883. [CrossRef]
15. Castorino, G.A.M.; Losi, E.; Manservigi, L.; Pinelli, M.; Spina, P.R.; Venturini, M. Energy and Economic Optimization of the Design and Operation of Hybrid Energy Plants Under Current and Future Economic Scenarios. In Proceedings of the ASME Turbo Expo 2024: Turbomachinery Technical Conference and Exposition, London, UK, 24–28 June 2024; ASME Paper No. GT2024-121980. [CrossRef]
16. Gimelli, A.; Iossa, R.; Karimi, A.; Muccillo, M.; Braccio, S.; Phan, H.T. Energy-saving and economic feasibility of a battery-integrated combined cooling, heating and power (CCHP) plant through waste heat recovery for H_2O-NH_3 based absorption, power and cooling (APC) system. *Energy* **2025**, *317*, 134640. [CrossRef]
17. Martelli, E.; Freschini, M.; Zatti, M. Optimization of renewable energy subsidy and carbon tax for multi energy systems using bilevel programming. *Appl. Energy* **2020**, *267*, 115089. [CrossRef]
18. Kiani-Moghaddam, M.; Soltani, M.N.; Weinsier, P.D.; Arabkoohsar, A. A bi-level, many-objective stochastic optimization model for handling simultaneous uncertainties in the operation of multi-carrier integrated energy systems: A hospital case study. *Sustain. Cities Soc.* **2025**, *127*, 106430. [CrossRef]
19. Castorino, G.A.M.; Dahlquist, E.; Kyprianidis, K.; Losi, E.; Manservigi, L.; Pinelli, M.; Renuke, A.; Spina, P.R.; Venturini, M. Optimization of sizing and operation of pumped hydro storage plants under current and future economic scenarios. *J. Energy Storage* **2025**, *119*, 116130. [CrossRef]
20. Castorino, G.A.M.; Losi, E.; Manservigi, L.; Pinelli, M.; Spina, P.R.; Venturini, M. Concurrent Design and Operation Optimization of a Multi-Generation Energy System by Using a SMO-MILP Hybrid Algorithm. In Proceedings of the ASME Turbo Expo 2023: Turbomachinery Technical Conference and Exposition, Boston, MA, USA, 26–30 June 2023; ASME Paper No. GT2023-101205. [CrossRef]
21. Qu, S.; Liu, F.; Cao, Z. An Adaptive Surrogate-Assisted Particle Swarm Optimization Algorithm Combining Effectively Global and Local Surrogate Models and Its Application. *Appl. Sci.* **2024**, *14*, 7853. [CrossRef]
22. An, Y.; Feng, B.; Li, M.; Gao, X.; Wang, H.; Li, J. Research on Peak-Valley Optimization of Distributed Photovoltaic Energy Storage Systems Based on an Improved Particle Swarm Algorithm. *Int. J. Thermofluids* **2025**, *30*, 101443. [CrossRef]

23. Hossain Lipu, M.S.; Ansari, S.; Miah, M.S.; Hasan, K.; Meraj, S.T.; Faisal, M.; Jamal, T.; Ali, S.H.M.; Hussain, A.; Muttaqi, K.M.; et al. A review of controllers and optimizations based scheduling operation for battery energy storage system towards decarbonization in microgrid: Challenges and future directions. *J. Clean. Prod.* **2022**, *360*, 132188. [CrossRef]
24. Bahlawan, H.; Losi, E.; Manservigi, L.; Morini, M.; Spina, P.R.; Venturini, M. Analysis of a Multi-Generation Renewable Energy System With Hydrogen-Fueled Gas Turbine. *J. Eng. Gas. Turbines Power* **2022**, *144*, 111020. [CrossRef]
25. Directive 2004/8/EC of the European Parliament and of the Council. Available online: https://eur-lex.europa.eu/legal-content/EN/TXT/PDF/?uri=CELEX:32004L0008 (accessed on 3 March 2025).
26. Carpinelli, M.; Macagno, S. *Monitoraggio Energetico Delle Strutture Sanitarie Pubbliche Regionali—Report 2023*; IRES Piemonte: Torino, Italy, 2023. (In Italian)
27. Carpinelli, M.; Macagno, S. *Monitoraggio Energetico Delle Strutture Sanitarie Pubbliche Regionali—Report 2024*; IRES Piemonte: Torino, Italy, 2024. (In Italian)
28. Decreto del Presidente Della Repubblica 26 Agosto 1993, n. 412. Available online: https://www.normattiva.it/uri-res/N2Ls?urn:nir:presidente.repubblica:decreto:1993;412 (accessed on 3 March 2025).
29. Michailidis, G.; Vavalos, P.; Kantzioura, A.; Zoras, S.; Dimoudi, A. Sustainability in the Healthcare Sector: Nearly Zero-Energy Building Strategies for Hospitals. *Energies* **2026**, *19*, 732. [CrossRef]
30. Ghiai, M.; Niknia, S. Energy and Sustainability Impacts of U.S. Buildings Under Future Climate Scenarios. *Sustainability* **2025**, *17*, 6179. [CrossRef]
31. Li, D.; Zhang, S.; Xiao, Y. Interval Optimization-Based Optimal Design of Distributed Energy Resource Systems under Uncertainties. *Energies* **2020**, *13*, 3465. [CrossRef]
32. Galletti S.p.A. Designing the Future: Galletti Catalogue 2024, Galletti S.p.A. [Online]. 2024. Available online: https://www.galletti.com/en/news/detail/Designing-the-future-with-the-new-Galletti-2024-catalogue (accessed on 3 March 2025).
33. Photovoltaic Geographical Information System (PVGIS)—European Commission. Available online: https://re.jrc.ec.europa.eu/pvg_tools/en/ (accessed on 3 March 2025).
34. Huld, T.; Paietta, E.; Zangheri, P.; Pinedo Pascua, I. Assembling Typical Meteorological Year Data Sets for Building Energy Performance Using Reanalysis and Satellite-Based Data. *Atmosphere* **2018**, *9*, 53. [CrossRef]
35. GME—Gestore Mercati Energetici. Available online: https://gme.mercatoelettrico.org/it-it/Home/Esiti/Elettricita/MGP/Esiti/PUN (accessed on 3 March 2025).
36. Piano Nazionale Integrato per L'energia e il Clima. Ministero dell'Ambiente e Della Sicurezza Energetica. Italia. Giugno 2024. Available online: https://www.mase.gov.it/portale/documents/d/guest/pniec_2024_revfin_01072024-pdf (accessed on 3 March 2025).
37. IEA. *World Energy Outlook 2024*; Licence: CC BY 4.0 (report); CC BY NC SA 4.0 (Annex A); IEA: Paris, France, 2024; Available online: https://www.iea.org/reports/world-energy-outlook-2024 (accessed on 3 March 2025).
38. IRENA. Renewable Power Generation Costs in 2022. 2023. Available online: https://www.irena.org/Publications/2023/Aug/Renewable-Power-Generation-Costs-in-2022 (accessed on 3 March 2025).
39. Yu, S.; Fan, Y.; Shi, Z.; Li, J.; Zhao, X.; Zhang, T.; Chang, Z. Hydrogen-based combined heat and power systems: A review of technologies and challenges. *Int. J. Hydrogen Energy* **2023**, *48*, 34906–34929. [CrossRef]
40. Bosh—Hydrogen Boilers. Bosch Industrial Boilers UK & Ireland. Available online: https://www.bosch-industrial.com/gb/media/country_pool/documents/bosch_hydrogen_boilers_print_version_.pdf (accessed on 24 June 2025).
41. Viessmann—100 Percent Hydrogen Operation Planned from 2025. Available online: https://www.viessmann-climatesolutions.com/en/hydrogen/100-percent-hydrogen-operation-planned-from-2025.html (accessed on 24 June 2025).
42. Mielich, T.; Rafael Dobler, R.; Hollnagel, J.; Akca, O.; Müller-Kirchenbauer, J. Europe's way from natural gas to green hydrogen: Modeling and simulation of the transforming European gas transport infrastructure. *Int. J. Hydrogen Energy* **2025**, *135*, 156–171. [CrossRef]
43. Neumann, F.; Zeyen, E.; Victoria, M.; Brown, T. The potential role of a hydrogen network in Europe. *Joule* **2023**, *7*, 1793–1817. [CrossRef]
44. IRENA—International Trade and Green Hydrogen, Supporting the Global Transition to a Low-Carbon Economy. World Trade Organization and International Renewable Energy Agency. 2023. Available online: https://www.irena.org/Publications/2023/Dec/International-trade-and-green-hydrogen-Supporting-the-global-transition-to-a-low-carbon-economy (accessed on 3 March 2025).
45. Robert, G.; Binder, C.; Wöll, S.; Roman, G.; Steffen, R. *Long Term (2050) Projections of Techno-Economic Performance of Large-Scale Heating and Cooling in the EU*; EUR 28859; Publications Office of the European Union: Luxembourg, 2017. [CrossRef] [PubMed]
46. Bahlawan, H.; Morini, M.; Spina, P.R.; Venturini, M. Inventory scaling, life cycle impact assessment and design optimization of distributed energy plants. *Appl. Energy* **2021**, *304*, 117701. [CrossRef]

47. Mongird, K.; Viswanathan, V.; Alam, J.; Vartanian, C.; Sprenkle, V.; Baxter, R. *2020 Grid Energy Storage Technology Cost and Performance Assessment*; U.S. Department of Energy: Washington, DC, USA, 2020. Available online: https://www.energy.gov/energy-storage-grand-challenge/downloads/2020-grid-energy-storage-technology-cost-and-performance (accessed on 3 March 2025).
48. Roychaudhuri, P.S.; Bandyopadhyay, S. Financial Pinch Analysis: Minimum opportunity cost targeting algorithm. *J. Environ. Manag.* **2018**, *212*, 88–98. [CrossRef] [PubMed]
49. Delapedra-Silva, V.; Ferreira, P.; Cunha, J.; Kimura, H. Methods for Financial Assessment of Renewable Energy Projects: A Review. *Processes* **2022**, *10*, 184. [CrossRef]
50. Saletti, C.; Conti, P.; Schito, E.; Morini, M.; Gambarotta, A.; Testi, D. Scenario-based assessment of electrification pathways in district multi-energy systems. *Energy* **2026**, *359*, 141479. [CrossRef]
51. Sun, Y.; Hu, Y.J.; Tao, Y.; Tang, B.J. Multi-energy complementary optimization for low-carbon public buildings with thermal comfort and time-of-use electricity constraints: Life-cycle cost-benefit and global sensitivity analysis. *Build. Environ.* **2026**, *291*, 114222. [CrossRef]
52. Eldakadosi, M.; Schneeloch, J. Hydrogen vs. conventional sector-coupling residential energy systems: An economic and environmental comparison based on multi-objective design optimization. *Renew. Energy* **2024**, *236*, 121412. [CrossRef]
53. Li, M.; Wang, M.; Shi, P.; Zhou, G.; Lu, Y. Techno-economic-environmental assessment and optimization of multi-energy complementary systems under dynamic building loads. *Energy* **2025**, *338*, 138935. [CrossRef]
54. Roncal-Casano, J.J.; Rodríguez-Martín, J.; Taddeo, P.; Muñoz-Antón, J.; Abánades-Velasco, A. Comparison of a Solar Driven Absorption Chiller and Photovoltaic Compression Chiller Under Different Demand Profiles: Technological, Environmental and Economic Performance. *Energies* **2025**, *18*, 5334. [CrossRef]
55. Tataraki, K.G.; Kavvadias, K.C.; Maroulis, Z.B. A systematic approach to evaluate the economic viability of Combined Cooling Heating and Power systems over conventional technologies. *Energy* **2018**, *148*, 283–295. [CrossRef]
56. Cauchi, G.; Magnini, S.; Danti, P. Thermal-electric decoupling approach for a medium-size CHP system: Electric storage vs thermal storage, economic comparison with different constraints. *Energy Procedia* **2018**, *148*, 559–566. [CrossRef]

Disclaimer/Publisher's Note: The statements, opinions and data contained in all publications are solely those of the individual author(s) and contributor(s) and not of MDPI and/or the editor(s). MDPI and/or the editor(s) disclaim responsibility for any injury to people or property resulting from any ideas, methods, instructions or products referred to in the content.